Thermodynamic Modeling of the Mg-Mn-(Al, Zn) Systems

Mohammad Asgar Khan

A Thesis
in
the Department
of
Mechanical and Industrial Engineering

Presented in Partial Fulfillment of the Requirements
for the Degree of Master of Applied Science (Mechanical Engineering) at
Concordia University
Montreal, Quebec, Canada

February 2009

Abstract

Thermodynamic Modeling of the Mg-Mn-(Al, Zn) Systems

Mohammad Asgar Khan

A self-consistent thermodynamic model of the Mg-Mn, Al-Mn, Mn-Zn binary systems as well as the Mg-Al-Mn and Mg-Mn-Zn ternary systems has been developed in the current work. The major difference with the already existing model of these systems is the application of the modified quasichemical model for the liquid phase in each system for which most of the existing descriptions use random mixing model. Further, this model is also used to describe one intermediate solid solution phase in the Mn-Zn system. In the absence of key experimental data for the Mg-Mn system, the calculated thermodynamic quantities from the model have been found comparable with other similar systems. The critical temperature of the Mg-Mn liquid miscibility gap has been estimated with the available empirical equation and found to be in acceptable agreement with the calculated value. The binary Al-Mn description has been found to be consistent with the existing reliable experimental data and other assessments. The Mn-Zn system has been modeled for the entire compositon range and wide temperature range starting from room temperature. The accepted experimental data are well reproduced with the current description of the Mn-Zn system. Kohler symmetric extrapolation model has been used to calculate both Mg-Al-Mn and Mg-Mn-Zn systems. The thermodynamic description of the Mg-Al-Mn system has been verified by extensive comparison with the available experimental data from numerous independent experiments. However, the calculated Mg-Mn-Zn system could not be thoroughly verified due to the lack of experimental data. The model can satisfactorily reproduce all the invariant points and the key phase diagram and

thermodynamic features of the Mg-Al-Mn, Mg-Mn-Zn ternary systems and the binary sub-systems.

Acknowledgements

I like to express my sincere gratitude to my supervisor, Dr. Mamoun Medraj, for his support and tireless effort in guiding me towards achieving my MASc degree in Concordia University. His cooperation and continuous inspiration made my stay here pleasant as well as fruitful.

I would like to thank Drs. Arthur Pelton , Patrice Chartrand and Youn-Bae Kang for their support and valuable suggestions which helped me a lot in understanding my work.

I thank all the members of the thermodynamics of materials research group of Dr. Medraj, especially, Sk. Wasiur Rahman and Mezbahul Islam for their help and support during my research.

I appreciate the support from my wife who sacrificed a lot and made this destination easily reachable. Without her sacrifice, it would have been very difficult indeed to finish the work in time. I also like to thank all my family members who were always a source of inspiration for me.

Finally the financial support from NSERC (Natural Sciences and Engineering Research Council of Canada) in carrying out this study is gratefully acknowledged.

Table of Contents

List of Figures

List of Tables

CHAPTER 1

Framework and Scope of the Current Work

1.1 Introduction

Mg-based alloys are being used extensively in many industries for producing different parts and equipments because of their better physical and mechanical properties compared to other metal alloys. Many different elements which include Al, Ca, Zn, Sr, Mn, Cu, Y etc. are alloyed with Mg to improve its properties for specific applications. A comprehensive and reliable thermodynamic database which includes these elements as constituents for Mg alloy system is thus an essential requirement for the better understanding of the system and predicting the system behavior in many practical applications such as design of experiments, solidification and heat treatment processes, etc. In essence, the existence of a reliable thermodynamic database enables the effective use of computational thermodynamics which have a significant potential to reduce the time, effort and money required to carry out numerous experiments and to replace them with only few key experiments. The present study deals with the thermodynamic modeling, within the CALPHAD framework, of the Mg-Al-Mn and Mg-Mn-Zn systems which are two of the most important parts of the desired multi-component Mg alloy database. These two ternary systems consist of five constituent binary systems namely Mg-Mn, Al-Mn, Mg-Al, Mg-Zn and Mn-Zn. Among these five binary systems Mg-Mn,

Al-Mn and Mn-Zn systems have been modeled in the current study and the other two binaries have been taken from [1,2]. The choice of the appropriate model for each of the stable phases in binary or higher order systems is one of the key steps in modeling a system in the well-known CALPHAD approach. Bragg-Williams model has been used to describe the liquid solution phase in most of the previous thermodynamic modeling of the Mg-Mn, Al-Mn, Mn-Zn, Mg-Al-Mn and Mg-Mn-Zn systems. In the present study, the Modified Quasichemical (MQC) model, as proposed by Pelton et al. [3], has been used to describe the liquid solution phases in the ternary as well as all the constituent binary systems. This model is used for describing the Mg-Mn-Zn system for the first time in the current work. The aim of this study is to present a thermodynamic description for the Mg-Mn, Al-Mn, Mn-Zn, Mg-Al-Mn and the Mg-Mn-Zn systems which can be combined to other existing databases like [4-8].

1.2 Objectives and Methodology

The ultimate purpose of this work is to develop a consistent thermodynamic database for the Mg-Al-Mn and the Mg-Mn-Zn systems. This implies finding a single set of model parameters for describing the Gibbs energy of each of the stable phases in every constituent binary system and the ternary systems which can describe all the reliable experimental phase diagram and thermodynamic data.

The well-known CALPHAD methodology has been followed in this regard. The key steps that have been followed in thermodynamic modeling of the two ternary systems and the binary subsystems have been shown in figure 1.1. A brief description of each of the steps of the framework has been given in the following sections:

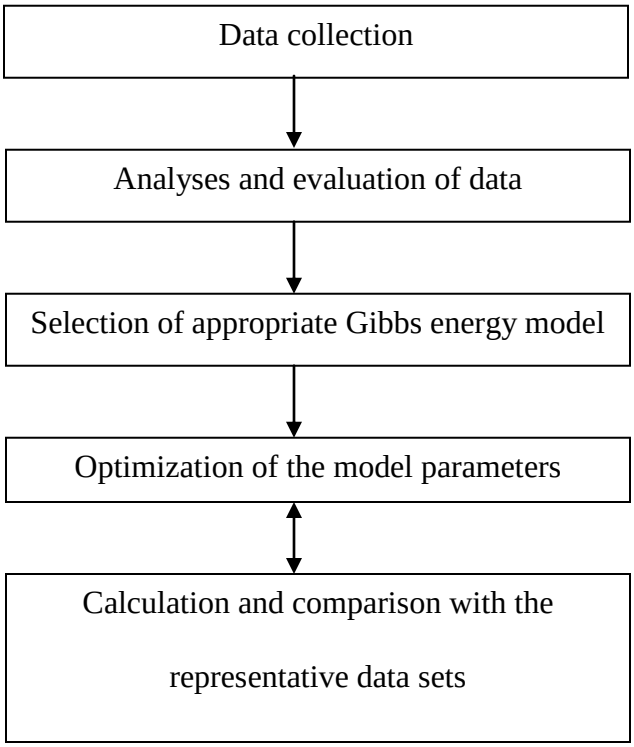

Fig 1.1 Key steps followed in the thermodynamic modeling of the Mg-Al-Mn and Mg-Mn-Zn systems

1.2.1 Data Collection

A diverse set of experimental data which represents the thermodynamic behavior of different phases in a system may be available in the literature. Extensive search has been carried out to collect the available information on the relevant binary and ternary systems. The types of information that have been searched for include experimental phase diagram data, type of phases present, type of invariant reactions occurring, thermodynamic properties of stoichiometric compounds, liquid and solid solution phases, melting temperatures, crystal structures, solubility, homogeneity range of different phases, experimental techniques and the possible sources and extent of errors, etc. The Gibbs energy expressions for each of the pure elements as well as all the previous assessments

of the intended binary and ternary systems have also been collected. All these information helps in establishing a comprehensive understanding of the thermodynamic features of the system under study which is the primary concern for beginning the thermodynamic modeling.

1.2.2 Analyses and Evaluation of Data

There are different types of experimental techniques for measuring different thermodynamic properties and phase diagram features. Each experimental technique itself and the method of measurement of a specific thermodynamic property have its own distinctive characteristics, merits and limitations. For example, the activity of a component in a binary solution phase can be measured by vapor pressure technique, EMF technique, mass spectrometric technique etc. The sources and the extent of error in these experiments depend on many interdependent factors like characteristics of the solution phase itself, sophistication of equipments, limits of detection of the equipment, reproducibility of results, purity of sample, expertise of the person carrying out the experiment etc. The second vital step in thermodynamic modeling is the evaluation of every single piece of experimental information by analyzing these factors together with the available earlier assessments in order to select the appropriate data sets for the optimization process. Different factors have been considered in evaluating the experimental data and some of the major factors are described briefly referring to some specific examples as follows:

- *Suitability of experimental technique*: Among the different available experimental techniques for measuring a specific thermodynamic property or phase diagram section, not all of them are suitable or appropriate. As one example, in the case

where a phase boundary of a temperature-composition phase diagram is steep, the fixed composition techniques (such as thermal analyses) may give rise to large error because of the weak signals generated by indistinguishable change in ΔCp values. However, fixed temperature technique (such as diffusion couple method) should give more accurate results in this case. Eventually, the data of Liu et al. [9] who used diffusion couple method for establishing the phase equilibria in the middle of the Al-Mn system has been selected following the suggestion of Liu et al. [10]. In the other case, the reliability of determining the joint solubility of Mn in Mg solid solution in the Mg-Mn-Zn system with microstructural observation by Bumazhnov [11] and Joel and Schneider [12] was questioned by Ohno and Schmid-Fetzer [13] due to its inherent measurement difficulties. Another issue is the structural characterization of different phases (e.g. whether X-ray diffraction (XRD) was used to confirm the presence of a phase or not). It is often crucial to accept an experimental result without extensive structural analysis of phases especially if there exists a large number of metastable phases in a system like Al-Mn binary. Many of the experimental results have been discarded in the assessment of the Al-Mn system by McAlister and Murray [14] because of the absence of structural characterization of the phases. Finally, the situation when contradictions are found between the heating and cooling data in the same experiment should be addressed. Usually, it is assumed that undercooling is more likely than overheating as pointed out in [10]. Thus the heating data of the liquidus in the Al-rich side of the Al-Mn system were preferred in this evaluation.

- Purity of sample used for experimental measurements: Mn containing alloys were not available with high purity until around 1970s [14]. Thus the experimental results obtained before 1970s may have significant errors. Many experimental data on Al-Mn system has been discarded in the assessment of McAlister and Murray [14] due to its probable sample impurities except for few of the consistent results.
- Attainment of equilibrium: The results that show evidence of reaching equilibrium (e.g. the time allowed for the equilibration) before taking the final reading is considered reliable. This is important for all the systems, especially for Al-Mn which shows very slow reaction rates [14]. In the assessment of Mg-Mn-Zn system, Ohno and Schmid-Fetzer [13] doubted the experimental results of Bumazhnov [11] on the ground that the equilibration time, he [11] allowed, might not be sufficient for the required solid state equilibria.
- Consistency with independent experiments: When similar results have been produced by two or more independent experiments, carried out by different experimental set-ups and different environmental settings, these results are considered as consistent and reliable and thus selected for comparison with the calculated values.
- Relative timing of experiments: It is likely that more recent data reflect more accurate results because of the likeliness of more understanding of the systems, more sophistication of equipments, techniques, software etc. with the progress of time. Thus, recently available data are generally preferred in the case of contradicting data. However, there are some cases where more recent data had to

be discarded because of some other factors described above. For instance, in the Al-Mn system, Mn-solubility data in the Al-rich side reported by Drits et al. [15] in 1964 was discarded because of the probability of having impurities but the older data reported by Dix et al. [16] in 1933, Butcher et al. [17] in 1945, Fahrenhorst et al. [18] in 1940 and Obinata et al. [19] in 1953 were taken as reliable because of their mutual consistency.

1.2.3 Choice of the Gibbs Energy Model

The third important step in the process of thermodynamic modeling as shown in figure 1.1 is to choose appropriate Gibbs energy model for each of the stable phases in a system. The choice of the model depends on some of the following key characteristics:

a) The model should represent the real thermodynamic features of the phase in a system. More speicifically, it should be able to account for the actual thermodynamic interactions at the atomic levels that cause the system exhibiting distinct features in the measured properties. For example, the short range ordering in a liquid phase or the long range interactions in a solid solution phase should be properly reflected in the chosen model.

b) The model should have good extrapolation ability. In other words, it should reliably predict the thermodynamic features in the higher order system which provides reasonable estimation of the thermodynamic properties.

c) Normally, simpler models are preferred in modeling different phases in a system. More complicated models which take care of the thermodynamic interactions more precisely are, generally, associated with higher degree of complexities. As an example, the entropy expression used for the modified quasichemical model is

based on the Ising approximation and provides fairly reasonable results; although the expression is only exact in one dimension [3]. Incorporating an exact two dimensional entropy expression in the model would definitely give more accurate prediction but involve huge complexities that may require unreasonable computer time, effort and calculation power. Thus, a balance should be made between the degree of sophistication and the degree of complexities when selecting the Gibbs energy model for a phase.

d) A good model usually involves physically significant parameters. For example, if a power series polynomial is used for describing the excess Gibbs energy function of a phase, it may require large number of parameters involving huge magnitude which might not have any physical significance. On the other hand, a Redlich-Kister type polynomial usually requires less number of parameters with the magnitude having physical significance. Thus, a Redlich-Kister type polynomial for the excess Gibbs energy function is often preferred.

More detailed description of the chosen models for different phases in the Mg-Al-Mn and Mg-Mn-Zn systems have been given in chapter 3.

1.2.4 Optimization of Model Parameters

The thermodynamic modeling and the optimization of model parameters have been carried out with the aid of the thermo-chemical software FactSage [20]. The parameters of the liquid phase have been optimized first to fit the experimental thermodynamic data. The other phases were then added systematically starting from terminal solution phases to the middle of the phase diagrams following the suggestions of Hari Kumar et al. [21]. For the Al-Mn system, the intermediate phase Al_8Mn_5 was kept as stoichiometric initially.

The excess Gibbs energy parameters were added one by one when necessity arises. When a reasonable agreement was achieved with the experimental phase equilibrium data, the Al_8Mn_5 was incorporated as solid solution and modeled with the necessary number of sublattices. All the parameters of the stable phases in the Al-Mn system were then fine-tuned simultaneously to optimize the system. The parameters of the binary Mg-Mn and Mn-Zn systems have been optimized in a similar approach. When the binary systems are optimized, they are then combined to extrapolate and calculate the ternary Mg-Al-Mn and Mg-Mn-Zn systems which are again optimized to reproduce the reliable experimental data if available.

1.2.5 Calculation and Comparison with the Representative Data

Optimization of model parameters is an iterative process. After every iteration step, the model parameters are used to calculate the phase equilibria and thermodynamic properties in each of the binary and ternary systems. The calculated values are then compared with the experimental data selected as reliable by careful evaluation as discussed in the previous section. The iteration continues until satisfactory agreement with all the reliable phase diagram data as well as the thermodynamic data has been achieved.

CHAPTER 2

Literature Review

2.1 Experimental Data and the Earlier Assessments

The available experimental information on the phase equilibria and thermodynamic properties of the Al-Mn, Mg-Mn, Mn-Zn, Mg-Al-Mn and Mg-Mn-Zn systems and the earlier assessments on these systems carried out by different group of researchers are discussed in the following sections.

2.2 Al-Mn System

Al-Mn binary phase diagram is characterized by a large number of stable phases in the system and this fact is established by numerous experimental investigations and thermodynamic assessments by many researchers. McAlister et al. [14] critically reviewed the experimental information on the Al-Mn system that were available prior to 1987 and provided their assessment on the system. Their assessed phase diagram for the Al-Mn system is shown in figure 2.1. Jansson [22] made some simplifications of the phase relationships of the Al-Mn system as compared to the assessed phase diagram of [14] and presented a thermodynamic description of the system throughout the entire composition region for the first time. Their [22] optimized Al-Mn phase diagram is shown in figure 2.2. However, the HCP phase in the Mn-rich side of the system was not correctly described by Jansson's model because of the probable inaccuracy of the

experimental data available at that time. Liu et al. [9] used more accurate fixed temperature technique (diffusion couple) for measuring such a steep phase boundary features and reported the phase equilibria data which were significantly different from the earlier available data. Based on their own experimental results, Liu et al. [10] re-modeled the Al-Mn system and their optimized phase diagram is shown in figure 2.3. Their [10] thermodynamic description of the system follows the observations of Okamoto [23] who suggested a smooth continuous liquidus curve for the same BCC phases separated by HCP phase. However, Liu et al. [10] did not include the experimental results of Müller et al. [24] who used Differential Thermal Analysis (DTA), optical microscopy, Scanning Electron Microscope (SEM) and XRD and reported the equilibrium liquidus and solidus curve for the HCP phase. However, Okamoto [23] included the data of [24] in their assessment of the Al-Mn system. Also, Liu et al. [10] did not consider the Mn solubility data of [25-28] as stated by [29]. Recently, Du et al. [29] re-modeled the Al-Mn system based on their own DTA, XRD, SEM and Energy Dispersive Spectrometry (EDS) results in the Al-rich side. They included the high temperature modification of the $Al_{11}Mn_4$ phase which was ignored in the previous modeling for lack of sufficient phase boundary data. Also, they [29] included the λ-Al_4Mn phase whose existence was questioned by Okamoto [23] due to its close proximity to μ-Al_4Mn. All the thermodynamic modeling of the Al-Mn system [10,22,29] discussed upto here were using the random solution model for the liquid phase. However, Shukla and Pelton [30] published a thermodynamic description of the Al-Mn and Mg-Al-Mn systems using the MQC model, which appeared recently after finishing the work on this thesis. The calculated results of their [30] work are compared with the current calculation in chapter 4.

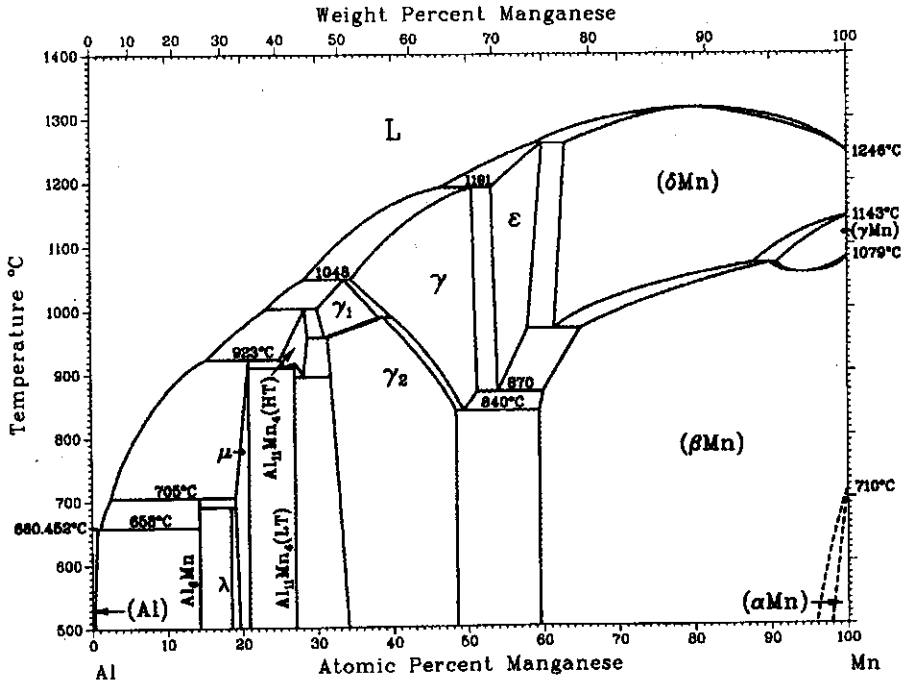

Fig 2.1 Al-Mn phase diagram assessed by [14]

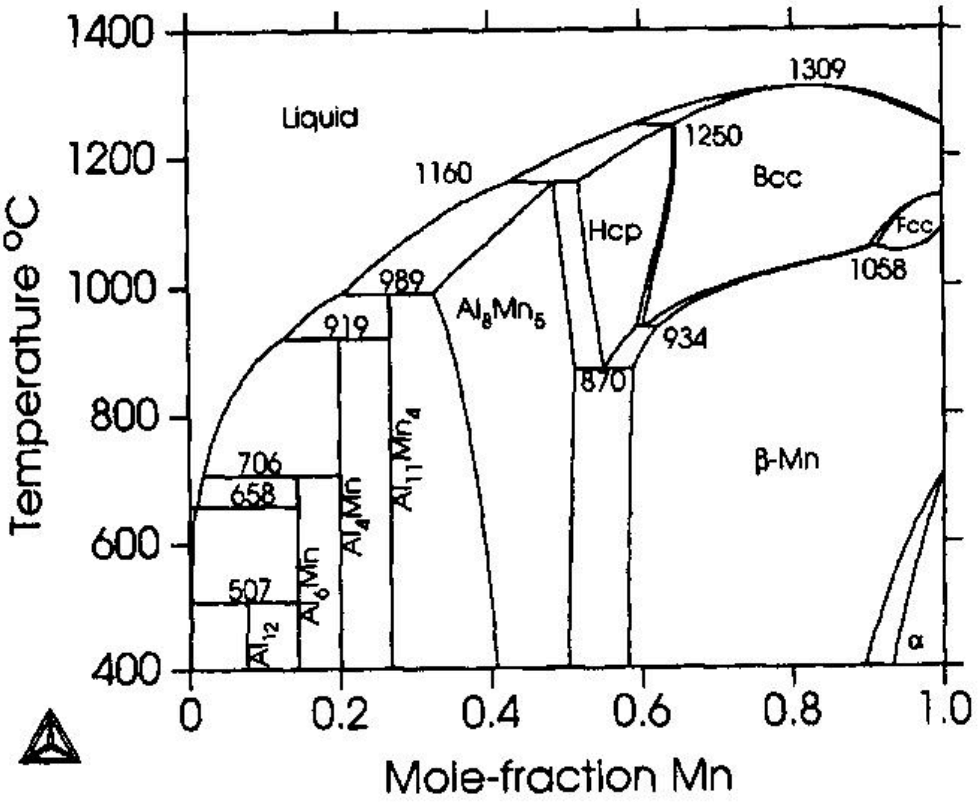

Fig 2.2 Al-Mn phase diagram optimized by [22]

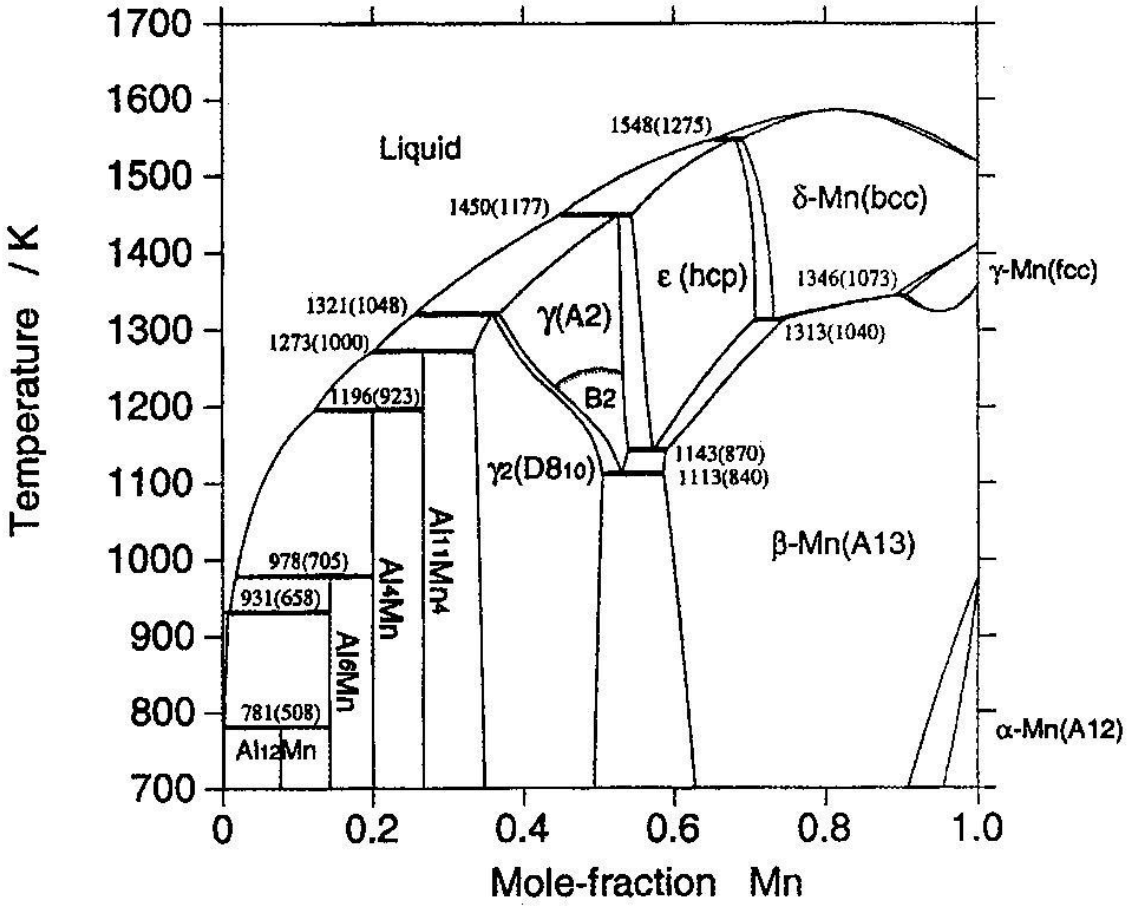

Fig 2.3 Al-Mn phase diagram optimized by [10]

The stable phases in the Al-Mn system, the existence of which are established by the experimental results and thermodynamic assessments of the previous researchers have been listed in table 2.1. The terminology and the models used in the current work in describing the Gibbs energy of all these phases are also shown in the table.

Table 2.1. Stable phases in the Al-Mn system and model used in the current work

System	Stable Phases	Description	As Modeled (current work)	Model used *
Al-Mn	(Al)	Terminal solid solution	Gamma (FCC)	SSM
	$Al_{12}Mn$	Stoichiometric	$Al_{12}Mn$	ST
	Al_6Mn	Stoichiometric	Al_6Mn	ST
	λ-Al_4Mn	Stoichiometric	-	Ignored
	μ-Al_4Mn	Compound with very limited solubility range.	Al_4Mn	ST
	$Al_{11}Mn_4$ (HT)	Compound with very limited solubility at high temperature	$Al_{11}Mn_4$	ST
	$Al_{11}Mn_4$ (LT)	Stoichiometric phase at low temperature	$Al_{11}Mn_4$	ST
	γ_1	Compound with considerable solubility range	Al_8Mn_5	CEF (Three Sublattice)
	γ_2	Compound with considerable solubility range	Al_8Mn_5	CEF (Three Sublattice)
	γ	Intermediate solid solution	Delta (BCC)	SSM
	ε	Intermediate solid solution	Epsilon (HCP)	SSM
	δ_{Mn}	Terminal solid solution	Delta (BCC)	SSM
	γ_{Mn}	Terminal solid solution	Gamma (FCC)	SSM
	β_{Mn}	Terminal solid solution	Beta (CUB)	SSM
	α_{Mn}	Terminal solid solution	Alpha (CBCC)	SSM

*CEF- Compound Energy Formalism, SSM- Substitutional Solution Model, ST- Stoichiometric compound

A number of experimental thermodynamic information is also available for the Al-Mn system. Esin [31] measured calorimetrically the enthalpy of mixing of liquid Al-Mn at 1353°C. Batalin [32] measured the activity of Al in liquid Al-Mn alloy at 1297°C by EMF measurement and Chastel et al. [33] measured the same at 1247°C using

Knudsen cell. Kubaschewski and Heymer [34] and Meschel and Kleppa [35] measured the enthalpy of formation of some of the solid Al-Mn alloys using, respectively, reaction calorimetry and direct synthesis calorimetry. Kematick and Myers [36] investigated the Al-Mn system using Knudsen cell-mass spectrometry and measured the activity of Al and Mn in some of the solid alloys at 902°C. All these data have been taken into consideration in the present assessment and compared with the current calculation.

2.3 Mg-Mn System

Mg-Mn system is characterized by a wide miscibility gap in the liquid. Very limited experimental data are available on this system and the available data are inconsistent among one-another. Most of the available data are on the Mg-rich side describing the limited solid solubility of Mn in Mg. Hashemi and Clark [37] critically assessed the experimental data available on this system and summarized the reliable data. They [37] did not find general agreement in the experimental results of [38-49] who investigiated only the Mg-rich portion of the Mg-Mn phase diagram. After analyzing the earlier assessments and the relatively more recent experimental works of [42-49], they [37] supported the existence of the peritectic type invariant reaction near Mg-rich region which was found to be the eutectic type in the experiments of [39-41] and Ishida [50]. The dip sampling techniques of measuring liquidus compositions followed by [39,44,46,47] was assessed to be prone to significant errors by [42] due to possible non-equilibrium effects and difficulties associated in determining the accurate composition. The liquidus lines reported by [48] were not in agreement with that of [47] which have been preferred by [37] who suggested that the higher liquidus temperatures were expected considering the sources of error in dip sampling technique. The mutual

solubility between Mn and Mg has been investigated by [40,42,44,46,47,49,51-54]. Hashemi and Clark [37] proposed a partial Mg-Mn phase diagram which was mainly based on the thermal analysis, microscopic observation and hardness measurements of [47] and the resistometric measurements of [49]. Their assessed diagram is shown in figure 2.4. The solubility data of Mn in Mg as determined by [44,46,54] are contradictory. Hence, in the present modeling, this solubility has been assumed negligible supported by the more recent experimental data of [54]. Although [41] reported an intermediate compound in the Mg-Mn binary system, it was not confirmed by the X-ray analyses of [46] and Bakhmetev and Golovchinev [55,56] as mentioned in [37]. The formation of an intermediate compound is also not expected in the binary Mg-Mn system considering the existence of large miscibility gap in the liquid which indicates that the atoms of Mg and Mn prefer to stay separate forming clusters. Gröbner et al. [57] examined the phase diagram at high temperature and reported a monotectic reaction temperature in the Mg-Mn system using the Differential Thermal Analysis (DTA) technique. They prepared sample with 99.97 wt% pure Mn and 99.98 wt% pure Mg and used specially adapted DTA equipment with sealed tantalum crucible. A cooling rate of 5K/min was employed for the DTA analyses and they calibrated the temperature using the melting point of high purity Ag, Al, Cu, In, Mg, Pb and Sb elements. In their experiment, the liquefied Mn was found to react with the Ta crucible to form the stable $TaMn_2$ which set some additional uncertainty on the measured monotectic temperature beyond the estimated overall uncertainty of ±3K. In addition to this experiment, they [57] modeled the system with the random solution model for the liquid phase based on their own results as well as previous experimental results on the Mg-rich side. Their model

calculates the consolute temperature of the liquid miscibility gap of the Mg-Mn system to be 4359°C [58]. Antion [59] questioned the existence of very high consolute temperature of the binary miscibility gap based on the experimental observation of the consolute temperature of the ternary Mg-Mn-Y system as discussed in [58]. Kang et al. [58] optimized the Mg-Mn system using the MQC model for the liquid phase with simultaneous consideration of the experimental data of [59]. Their optimization results in a consolute temperature of Mg-Mn liquid miscibility gap to be 1902°C which is much lower than that of the earlier model of Gröbner et al. [57]. In the absence of key experimental information in the lower order system, especially, when contradicting results are found by different independent assessments like in [57,58], it is interesting to compare the thermodynamic properties with similar binary systems. Although this is not as accurate as comparing with experimental data, this procedure will provide guidelines for the trends and order of magnitude of the needed thermodynamic properties.

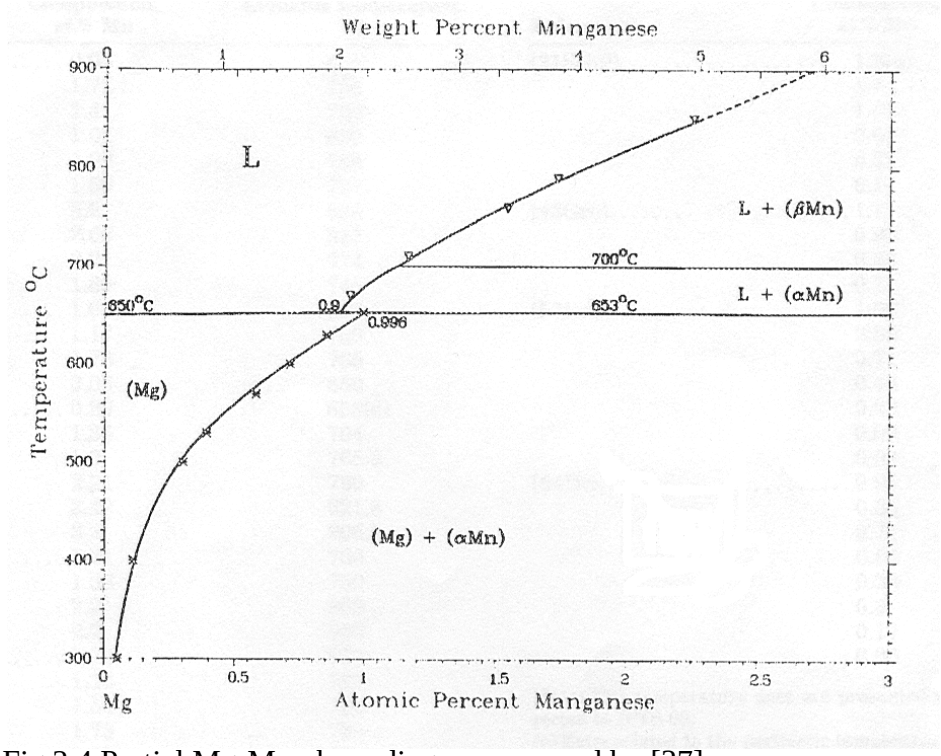

Fig 2.4 Partial Mg-Mn phase diagram assessed by [37]

The stable phases in Mg-Mn system, the existence of which are established by the experimental results and thermodynamic assessments of the previous researchers have been listed in table 2.2. The terminology and the models used in the current work in describing the Gibbs energy of these phases, except the liquid phase, are also shown in the table.

Table 2.2 Stable phases in the Mg-Mn system and the models used in the current work

System	Stable Phases	Description	As Modelled (current work)	Model used *
Mg-Mn	α_{Mn}	Terminal solid solution	Mn (CBCC)	ST
	β_{Mn}	Terminal solid solution	Mn (CUB)	ST
	γ_{Mn}	Terminal solid solution	Gamma (FCC)	SSM
	δ_{Mn}	Terminal solid solution	Delta (BCC)	SSM
	(Mg)	Terminal solid solution	HCP	SSM

* SSM- Substitutional Solution Model, ST- Stoichiometric compound

2.4 Mn-Zn System

Numerous researchers have investigated the Mn-Zn system experimentally in order to establish the phase equilibria and thermodynamic aspects of the system. Many of these experimental results contradict with one another. Okamoto and Tanner [60] rigorously reviewed and summarized the earlier experimental works of [61-95] on the phase equilibria, thermodynamic properties and the crystal structures of different phases in the Mn-Zn system which were available prior to 1980. Their [60] assessed Mn-Zn phase diagram was based primarily on the phase equilibria data of Wachtel and Tsiuplakis [89] for the composition range 60 to 100 at. % Zn, on Romer and Wachtel [93] for 0 to 60 at. % Zn above 400°C and on Nakagawa and Hori [81] for the 30 to 70 at. % Zn below 400ºC. Their [60] assessed diagram is shown in figure 2.5.

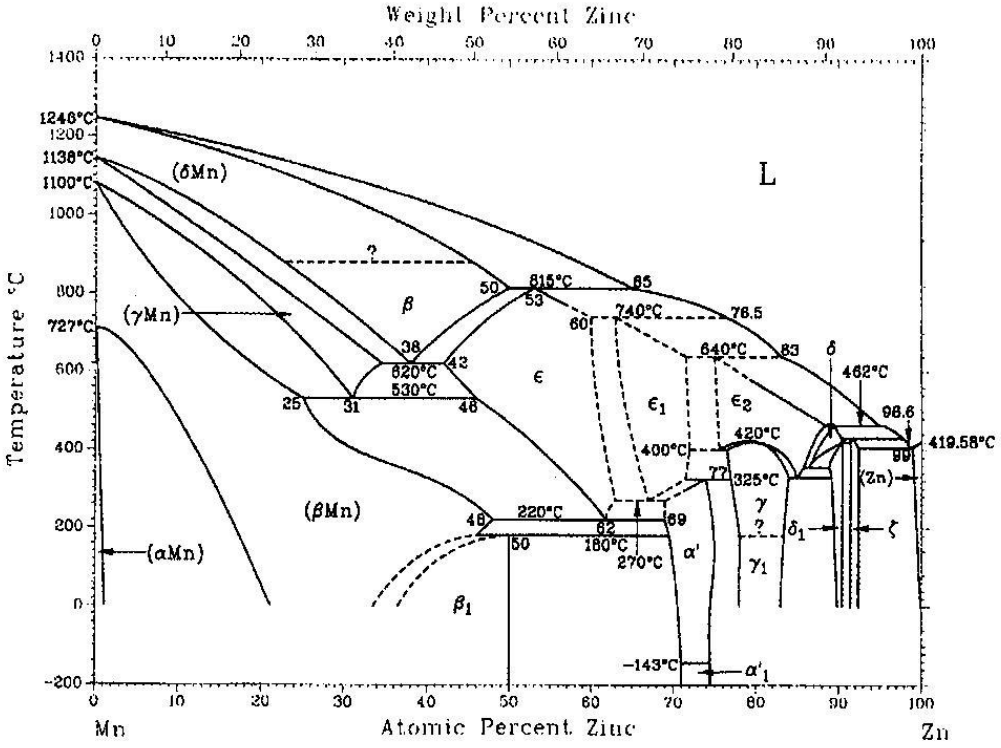

Fig 2.5 Mn-Zn phase diagram assessed by [60]

Miettinen [96] modeled the Mn-Zn binary system using the experimental data recommended by Okamoto and Tanner [60]. His [96] optimized Mn-Zn system is shown in figure 2.6. He [96] used random mixing model for the binary liquid phase and optimized the system above 400ºC. In the Mn-rich part of the system, he could not achieve good agreement with the experimental data of [93] who observed wider two solid phase regions of Alpha (CBCC) and Beta (CUB).

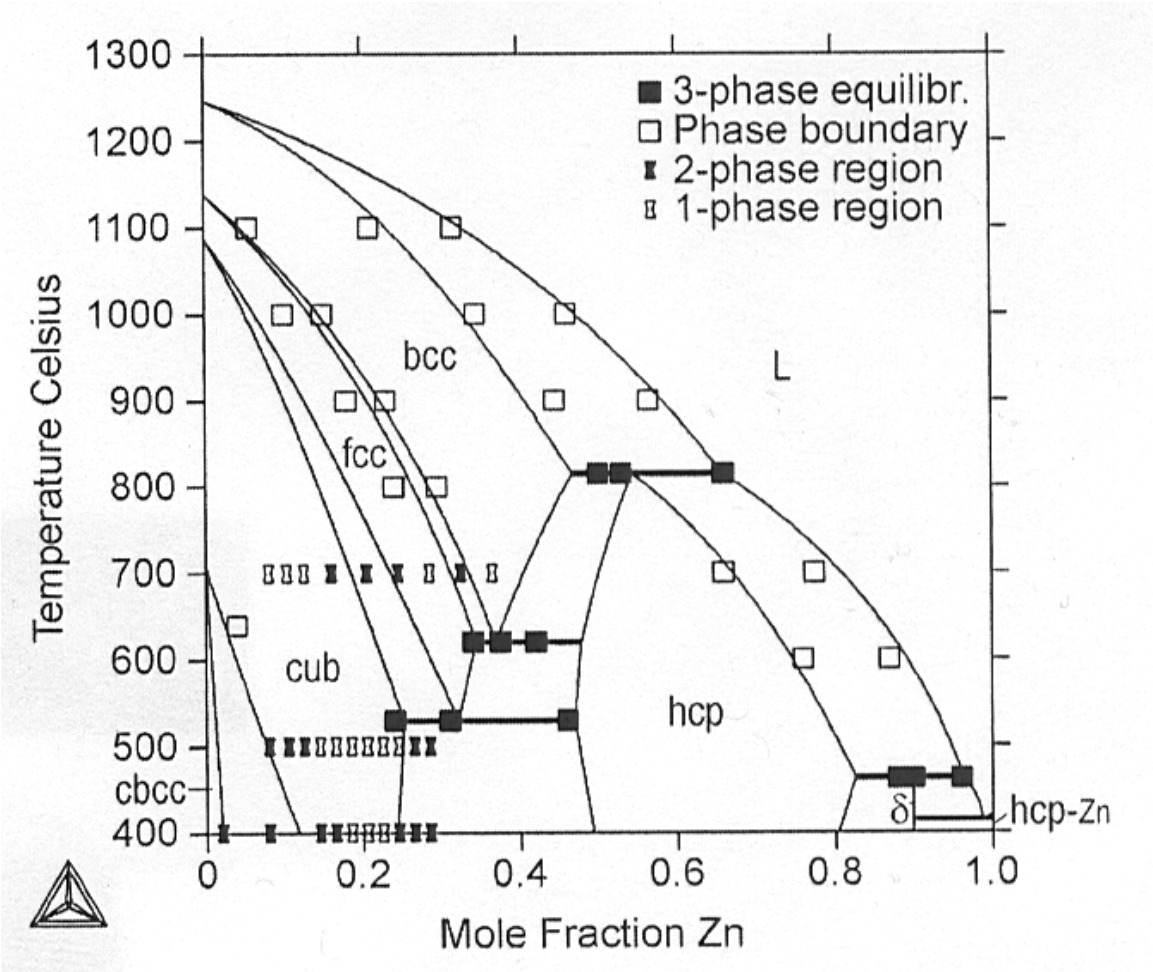

Fig 2.6 Mn-Zn phase diagram as optimized by [96]

The stable phases in the Mn-Zn binary system have been listed in table 2.3. The terminology and the models used in the current work in describing the Gibbs energy of all these phases are also shown in the table.

Table 2.3. Stable phases in the Mn-Zn system and the models used in the current work

System	Stable Phases	Description	As Modelled (current work)	Model used *
Mn-Zn	α_{Mn}	Terminal solid solution	Alpha (CBCC)	SSM
	β_{Mn}	Terminal solid solution	Beta (CUB)	SSM
	γ_{Mn}	Terminal solid solution	Gamma (FCC)	SSM
	δ_{Mn}	Terminal solid solution	Delta (BCC)	SSM
	(Zn)	Terminal solid solution	HCP	SSM
	ε	Intermediate solid solution	Epsilon (HCP)	MQC
	ε_1	Intermediate solid solution	Epsilon (HCP)	MQC
	ε_2	Intermediate solid solution	Epsilon (HCP)	MQC
	ζ	Compound with very limited solubility range.	$Zn_{13}Mn$	ST
	δ	Compound with very limited solubility range.	Zn_9Mn	ST
	δ_1	Compound with very limited solubility range.	Zn_9Mn	ST
	γ	Compound with limited solubility range.	Zn_8Mn_5	CEF (Two Sublattice)
	γ_1	Compound with limited solubility range.	Zn_8Mn_5	CEF (Two Sublattice)
	α'	Compound with limited solubility range.	Zn_3Mn	ST
	β_1	Compound with limited solubility range.	ZnMn	ST

*CEF- Compound Energy Formalism, SSM- Substitutional Solution Model, ST- Stoichiometric compound

2.5 Mg-Al-Mn System

Many researchers [29, 97-111] investigated the phase equilibria of the ternary Mg-Al-Mn system. All the experimental data are available near the Mg-Al edge of the ternary system. No experimental information on the Mn rich corner of the ternary was found in the literature. Ohno and Schmid-Fetzer [97] briefly reviewed the earlier experimental findings of [43,98-103] some of which [99,101-103] have been elaborated here for the better understanding of the system. Nelson [99] determined the liquidus and solidus surface of the Mg-Al-Mn system at the Mg-rich corner. He used metallographic examination of quenched samples together with stress-rupture upon incipient melting techniques for the determination of solidus and settling technique for determining the liquidus curves. He observed that the solubility of manganese was greatly depressed by the addition of small amount of aluminum and further decreased with increasing amount of aluminum in the alloys. Simensen et al. [102] investigated the phase equilibria in molten Mg-4wt% Al-Mn alloys. They used centrifugal and rapid quenching technique for preparing the sample and XRD, emission spectrometer and microprobe for microstructure analyses. They [102] found the solubility of manganese increasing rapidly with temperature as their microprobe analyses of rapidly quenched samples revealed. They also found that the equilibrium phase at this composition was Beta (CUB) above 720°C and the Al_8Mn_5 phase below 720°C although the exact transition temperature was mentioned to be uncertain. However, some of their samples contained significant iron impurities which might stabilize unexpected phases as they interpreted. The same group [101] also determined the ternary phase diagram near the Mg-rich corner between 660°C and 760°C. They [101] used the same techniques as in [102] for the sample preparation

and analyses. They observed Beta (CUB), Al_8Mn_5 and $Al_{11}Mn_4$ phases successively in equilibrium in the magnesium melts with composition increasing from 0.8wt% to 10 wt% aluminum. Beta (CUB) was found to be stable in melts containing 0.8 wt% Al and 4.0 wt% Al held above 730°C. Al_8Mn_5 was the main intermetallic phase from 4 wt% Al to 10 wt% Al and $Al_{11}Mn_4$ was the equilibrium phase below 670°C in Mg-10 wt% Al-Mn alloy. They concluded that the solubility of manganese increases with decreasing concentration of aluminum and with increased temperature supporting the experimental observations of [43,99,102] and verified by the most recent experimental works by Thorvaldsen and Aliravci [103]. However, Ohno and Schmid-Fetzer [97] found a significant quantitative disagreement in these observations. They [103] also measured the solubility of manganese in liquid Mg-Al alloys at various temperatures ranging from 600 to 750°C. They [103] prepared samples at 770-800°C by adding high purity aluminum and $MnCl_2$ to the commercial pure magnesium melt and reduced the temperatures stepwise at a high rate (maximum 10°C per min) by air cooling. The melt samples were held for a minimum of 45 minutes at the holding temperatures of 730, 700, 670, 640 and 610°C. At the end of holding periods they [103] cast the samples directly from the crucible into another permanent mould from which all the specimens for chemical analyses were taken. Their sample preparation and analyses procedure is unlike most other similar experimental investigations where either a relatively low temperature reduction rate was followed or the sample was contaminated with iron impurities (>.002 wt%) possibly causing significant error as stated by [103]. They [103] analyzed all samples by both emission spectrometry and Induction Coupled Plasma (ICP). Comparative analyses of all the earlier experimental investigations on the solubility of

Mn in Mg-Al alloys in terms of the sophistication of the measurement techniques, possible sources and extent of errors, consistency with the other independent experiments, relative timing of the experiments etc. indicates that the quantitative result of Thorvaldsen and Aliravci [103] is possibly more accurate than that of the others. However, the data of Nelson [99], Mirgalovskaya [100], Siemensen et al. [101,102] and Thorvaldsen and Aliravci [103] which were evaluated as reliable by Ohno and Schmid-Fetzer [97] are compared with the current calculation for the Mg-rich corner of the Mg-Al-Mn system. Ohno and Schmid-Fetzer [97] presented the thermodynamic modeling of the Mg-Al-Mn system focusing on the Mg-rich part of the system. On the other hand, Du et al. [29] reassessed the Al-Mn binary system based on their own experimental data at the Al-rich side and presented the thermodynamic model for the ternary Mg-Al-Mn system for the entire composition range. They [29] reviewed the previous experimetnal investigations on the Al-rich part of the ternary system and compared the data of Fahrenhorst et al. [18], Wakeman and Raynor [108] and Ohnishi et al. [109,110] with their calculated results because of the consistency of these data. The current calculations are also compared with these data [19,108-110] for the Al-rich part of the Mg-Al-Mn system. It is worth mentioning here that these two previous modeling on the ternary Mg-Al-Mn system [29,97] have been done using the random solution model for the liquid phase.

2.6 Mg-Mn-Zn System

Only two experimental measurements on the Mg-Mn-Zn phase equilibria have been found in the literature. Raynor [112] provided a brief review on the work of Joel and Schneider [12] and Bumazhnov [11]. Ohno and Schmid-Fetzer [13] reviewed these works

and only the key aspects are summarized here. Bumazhnov [11] measured the solubility of Mn and Zn in Mg solid solution by microstructural analyses and XRD measurements. He observed a significant increase in Mn solubilitiy in Mg solid solution with decreasing amount of Zn. Joel and Schneider [12], on the other hand, studied the ternary phase equilibria in the Mg-rich region which was found only qualitatively consistent with the work of Bumazhnov [11] by Ohno and Schmid-Fetzer [13]. They [13] also presented a thermodynamic description of the Mg-Mn-Zn system which agrees with none of the two available experimental data of [11,12]. Ohno and Schmid-Fetzer [13] disputed the results of Bumazhnov's [11] experiment on the ground that the 30 days annealing period and the subsequent isothermal holding for 7 days at different temperatures may not be sufficient for the required solid state equilibrium in the Mg-rich corner of the Mg-Mn-Zn system. Also, the technique of microstructural observation in detecting the solubility limit of Mn in Mg solid solution in Mg-Mn-Zn system was criticized by [13] for its inherent difficulties. Further, the ternary invariant reaction in the Mg-rich region of the Mg-Mn-Zn system depicted by Joel and Schneider [12] was correctly assessed to be thermodynamically unreasonable in [13]. Thus the data of Joel and Schneider [12] is ignored and the current calculation is only compared with the data of Bumazhnov [11].

CHAPTER 3

Thermodynamic Modeling and Description of the Models

3.1 Thermodynamic Modeling

The Gibbs energy of any system is expressed as G = H – TS, where, H, T and S are the enthalpy, entropy and temperature respectively. A system at constant temperature and pressure will be in an equilibrium state that corresponds to the minimum G. For a system, where, the pure compounds A, B, C and the solution phases α, β, γ are present in equilibrium, the total Gibbs energy may be written as:

$G = (n_A g_A^0 + n_B g_B^0 + n_C g_C^0) + (n_\alpha g_\alpha + n_\beta g_\beta + n_\gamma g_\gamma)$ where, g_i^0 are the molar Gibbs energies of the pure compounds, g_i are the molar Gibbs energies of the solution phases and n_i represents the number of moles of each of the phases. Thermodynamic modeling deals with finding the values of the set of number of moles $n_A, n_B, n_C \ldots\ldots\ldots n_\alpha, n_\beta, n_\gamma$ as well as the compositions of all phases which minimizes the total Gibbs energy *G* under the given set of constraints (such as fixed temperature, pressure and overall composition). The Gibbs energy for each of the phases g_α are represented as functions of composition and temperatures by various solution models the parameters of which are optimized using Gibbs energy minimization programs incorporated in a software like FactSage [20]. These optimized parameters for the lower order systems are stored in a multicomponent database which can be used to

predict the thermodynamic behavior of multicomponent systems [113]. The following sections describe the model used for each of the phases in the Mg-Mn, Al-Mn, Mn-Zn, Mg-Al-Mn and Mg-Mn-Zn systems in detail.

3.2 Pure Elements

Gibbs energy of a pure element (i) in a phase (ϕ) is represented by the equation

${}^{0}G_i^{\phi}(T) = G_i^{\phi}(T) - H_i^{SER}$ and

$$G_i^{\varphi} = a + bT + cT\ln T + dT^2 + eT^3 + fT^{-1} + gT^7 + hT^{-9}$$

Where, H_i^{SER} is the molar enthalpy of stable element reference (SER) at a temperature of 298.15K and at 1 atm pressure. In the current work, the stable phases at room temperature, i.e. HCP for Mg, FCC for Al, CBCC for Mn and HCP for Zn are selected as the reference phases. The parameters, *a* to *h*, of the Gibbs energy function for the pure elements in each phase has been taken from Dinsdale [114] except for the Zn (CBCC) and Zn (CUB) phase. As the parameters for pure Zn in these two metastable phases are not available in the literature, they have been optimized in the current work.

3.3 Liquid Phases

The liquid solution phases in the Mg-Mn, Al-Mn, Mn-Zn, Mg-Al, Mg-Zn, Mg-Al-Mn and Mg-Mn-Zn systems have been modeled with the MQC model. Since the major contribution of the current work is to use the MQC model for the liquid instead of Bragg-Williams (BW) (i.e. random-mixing) model, it may be worthwhile to compare the two models in light of the discussions reported by [115]. In BW model, the constituent atoms are assumed to be distributed randomly over the sites of a quasilattice to obtain the expression for the configurational entropy. The enthalpy of mixing is expressed as a

parabolic function $\Delta H = X_A X_B \omega_{BW,}$ where, $X_A X_B$ is the probability that a nearest neighbor pair is an (A-B) pair which is also equal to the probability that the n^{th} nearest neighbor pair is an (A-B) pair in a random mixture. This type of parabolic expression is not well suited for the V-shaped enthalpy of mixing curves which is typical for liquid phases with strong short range ordering. The BW term ω_{BW} is often expanded as a polynomial of Redlich-Kister type. Although the typical V-shaped enthalpy of mixing curve can be closely reproduced using several BW parameters, the partial properties may be in great error in the dilute solution region as pointed out in [115]. Also, the characteristic m-shaped entropy of mixing curve can only be generated with an additional independent parabolic expression for the entropy of mixing with several empirical parameters. Further, BW model often overestimates the tendency to liquid immiscibility in the ternary solutions, especially if one of the binaries shows much stronger tendency to short range ordering than the other two binaries. This is because the strong short range order in one of the binaries, which ultimately decreases the driving force to separate into two phases in the ternary solutions, has been ignored in BW model [115].

On the other hand, MQC model is, actually, a modification of the classical quasichemical model as proposed by Pelton et al. [3]. The detailed description of the MQC model is given in [3] and only key aspects of the model are briefly discussed in this section.

The governing equation for this model is:

$$\Delta g_{AB} = \Delta g^{o}_{AB} + \sum_{i \geq 1} g^{i0}_{AB} X^{i}_{AA} + \sum_{j \geq 1} g^{0j}_{AB} X^{j}_{BB}$$

where, Δg_{AB} is the change in the Gibbs energy for the formation of 2 moles of A-B pair from one mole of (A-A) and one mole of (B-B) pair according to the pair exchange reaction (A-A) + (B-B) = 2(A-B). A and B denote the atoms of the elements which are distributed over a quasilattice. The X_{AA} is the pair fractions defined as the ratio of the number of moles of (A-A) pairs to the total number of moles of (A-A), (B-B) and (A-B) pairs. The $\Delta g^{o}_{AB}, g^{i0}_{AB}$ and g^{0j}_{AB} are the parameters of the model to be optimized and may be temperature dependent. It is to be noted here that unlike the BW model, the configurational entropy is approximated in MQC model by randomly distributing the pairs over the 'pair sites' in a one dimensional lattice. The coordination numbers Z_A and Z_B of atoms A and B are permitted to vary according to the following equations:

$$\frac{1}{Z_A} = \frac{1}{Z^A_{AA}}\left(\frac{2n_{AA}}{2n_{AA}+n_{AB}}\right) + \frac{1}{Z^A_{AB}}\left(\frac{n_{AB}}{2n_{AA}+n_{AB}}\right)$$

$$\frac{1}{Z_B} = \frac{1}{Z^B_{BB}}\left(\frac{2n_{BB}}{2n_{BB}+n_{AB}}\right) + \frac{1}{Z^B_{BA}}\left(\frac{n_{AB}}{2n_{BB}+n_{AB}}\right)$$

where, All Z^i_{ii} is the coordination numbers of atom *i* when the surrounding atoms are similar and Z^i_{ij} is the coordination numbers of atom *i* when the surrounding atoms are dissimilar. The model can also be used for solid solutions with only exception that the coordination numbers are essentially restricted according to $Z^i_{ii} = Z^i_{ij}$. As such, in the current work, the MQC model has been used for modeling the intermediate solid solution, epsilon (HCP) phase, in the Mn-Zn system.

The major advantage of the MQC model is that it expands the Gibbs energy function of the solution phase in terms of pair fractions instead of equivalent fractions which results in greater flexibility in optimizing the parameters for the systems,

especially for those showing a large degree of short range ordering in the liquid [3]. It is physically more realistic in a sense that it considers the preferential formation of nearest neighbor A-B pairs for the short range ordering. It allows choosing freely the composition of the maximum short range ordering in the liquid in the binary system by choosing a suitable composition dependent coordination number. Successful application of this model for the optimization of numerous binary and higher order systems justifies choosing this model for optimizing the current systems as a part of developing a multicomponent database. The choice of the MQC model for the liquid phases leads to the required consistency with the other existing databases [4-8], developed with the same model for Mg alloys.

3.4 Terminal Solid Solutions

The crystal structure and homogeneity range data of differenct phases [14,37,60,116] indicate the formation of substitutional solid solutions for the terminal solid solutions in all the three binary systems. Thus a substitutional solution model (SSM) which allows complete mixing of the pure atoms on the same lattice has been used for these phases. The Gibbs energy, per mole of the phase (ϕ) for the A-B binary system is given by:

$$\Delta G^{\phi} = x_A {}^{o}G_A + x_B {}^{o}G_B + RT\left(x_A \ln x_A + x_B \ln x_B\right) + {}^{ex}G^{\phi}$$

where the excess Gibbs energy ${}^{ex}G^{\phi}$ for the phase (ϕ) is given by

$${}^{ex}G^{\phi} = x_A x_B \left[{}^{0}L^{\phi}_{A,B} + \left(x_A - x_B\right)^{1} L^{\phi}_{A,B} + \left(x_A - x_B\right)^{2} {}^{2}L^{\phi}_{A,B} \right]$$

where each of the L terms may be temperature dependent according to

$${}^{n}L^{\phi}_{A,B} = C + DT$$

where C and D are the parameters to be determined during the optimization process.

3.5 Stoichiometric Phases and Intermediate Solid Solutions

Modeling of the stoichiometric and near stoichiometric phases in all the binaries Mg-Mn, Al-Mn and Mn-Zn and the ternary Mg-Al-Mn systems have been carried out with compound energy formalism with sublattices having only pure elements in each of the sublattices without any mixing. This model is termed as stoichiometric (ST) model here. The Gibbs energy of formation for the stoichiometric phases is given by:

$$\Delta G_{A_pB_q} = {}^{o}G^{A_pB_q} - p\,{}^{o}G_A^{(A)} - q\,{}^{o}G_B^{(B)} = C + DT$$

where p and q are the site fractions in the two sublattices of the compound A_pB_q and the C and D values are to be optimized using experimental data.

The intermediate solid solutions in the Al-Mn and Mn-Zn systems have been modeled taking into account the crystal structure data and the experimental solubility range according to the suggestions of Hari Kumar et al. [117]. The intermediate Al_8Mn_5 phase in Al-Mn system has been simplified to three sublattices as suggested by Jansson [22] and as verified by the crystal structure data of its prototype Al_8Cr_5 [116]. The Gibbs energy of this phase for 13 moles of atoms is given by:

$$\begin{aligned}\Delta G^{Al_8Mn_5} = {} & y_{Al}\,{}^{o}G_{Al:Mn:Al} + y_{Mn}\,{}^{o}G_{Al:Mn:Mn} + 5RT\left(y_{Al}\ln y_{Al} + y_{Mn}\ln y_{Mn}\right) \\ & + y_{Al}y_{Mn}\left[{}^{o}L_{Al,Mn} + \left(y_{Al} - y_{Mn}\right){}^{1}L_{Al,Mn}\right]\end{aligned}$$

where, y_{Al} and y_{Mn} are the site fractions on the third sublattice of Al and Mn, respectively. The formation Gibbs energy of the end members ${}^{o}G_{Al:Mn:Al}$ and ${}^{o}G_{Al:Mn:Mn}$ and the L terms are optimized to fit the experimental data. The relations between the mole fractions and site fractions are given by $X_{Al} = \frac{6+5y_{Al}}{13}$ and $X_{Mn} = \frac{2+5y_{Mn}}{13}$, where, X_{Al} and X_{Mn} are the mole fractions of Al and Mn, respectively.

Similar analysis has been performed for modeling the intermediate solid solution Zn_8Mn_5 phase in the Mn-Zn binary system. Two sublattices have been taken with only Zn in the second sublattice with 8 sites and mixing both Mn and Zn atoms on the first sublattice with 5 sites. The Gibbs energy of this phase for 13 moles of atoms is given by:

$$\Delta G^{Zn_8Mn_5} = y_{Zn}\,{}^{o}G_{Zn:Zn} + y_{Mn}\,{}^{o}G_{Mn:Zn} + 5RT\left(y_{Zn}\ln y_{Zn} + y_{Mn}\ln y_{Mn}\right) + y_{Zn}y_{Mn}\,{}^{o}L_{Mn,Zn}$$

where, y_{Zn} and y_{Mn} are the site fractions on the first sublattice of Zn and Mn, respectively. The formation Gibbs energy of the end members ${}^{o}G_{Zn:Zn}$ and ${}^{o}G_{Mn:Zn}$ and the L terms are optimized to fit the experimental data. The relations between the mole fraction and site fraction are given by $X_{Zn} = \frac{8+5y_{Zn}}{13}$ and $X_{Mn} = \frac{5\,y_{Mn}}{13}$, where X_{Zn} and X_{Mn} are the mole fractions of Zn and Mn, respectively.

The other intermediate solid solution phases Epsilon (HCP) and Delta (BCC) in the Al-Mn system have been modeled with the substitutional solution model based on their crystal structure information [23,60,118].The intermediate solid solution Epsilon (HCP) in the Mn-Zn system has been modeled with MQC model as described earlier. The pure Mn CBCC and CUB phases in the Mg-Mn binary system have also been modeled as stoichiometric phases in this work.

CHAPTER 4

Results and Discussions

4.1 Results and Discussions

The process of the current thermodynamic modeling results in a set of model parameters that describe the Gibbs energy function of all the phases in the Mg-Mn, Al-Mn, Mn-Zn, Mg-Al-Mn and Mg-Mn-Zn systems. The optimized parameters for all the binary phases in the Al-Mn, Mn-Zn, Mg-Mn and Mg-Al-Mn systems are listed in tables 4.1 through 4.2, 4.3 and 4.4, respectively. The values of the composition dependent coordination numbers used in the MQC model for all the atoms in different phases have been chosen to be 6 except for the coordination number of the Mg-Mn pairs, designated as Z_{MgMn}^{Mg}, which has been chosen to be 4. This choice of the hypothetical coordination numbers ensures the required consistency with the other existing databases [4-8] on one hand while giving the best description of the systems. The notion for the best description of a system is associated with the capability of the model parameters to consistently reproduce the reliable experimental phase equilibria and thermodynamic data.

Table 4.1 The optimized parameters of the stable phases in the Al-Mn system

Phase	Model *	Parameters	**C** (J/mol atom)	**D** (J/mol atom K)
Liquid	MQC	${}^{o}L$	-18 367.76	6.527
		${}^{1}L$	-7 154.64	2.761
$Al_{12}Mn$	ST	$\Delta G_{Al_{12}Mn}$	-8 400.38	2.597
Al_6Mn	ST	ΔG_{Al_6Mn}	-15 124.29	4.227
Al4Mn	ST	ΔG_{Al_4Mn}	-20 590.00	5.621
$Al_{11}Mn_4$	ST	$\Delta G_{Al_{11}Mn_4}$	-22 246.67	4.664
Alpha (CBCC)	SSM	${}^{o}L$	-79 106.89	40.627
		${}^{1}L$	-14 476.64	0.0
Gamma (FCC)	SSM	${}^{o}L$	-44 275.09	3.556
Epsilon (HCP)	SSM	${}^{o}L$	-1 01 708.86	36.07
		${}^{1}L$	-8 280.14	5.146
		${}^{2}L$	1 32 758.32	-83.178
Delta (BCC)	SSM	${}^{o}L$	-1 22 800.40	51.04
		${}^{1}L$	67 362.40	-41.171
Al_8Mn_5	CEF, three sublattices	${}^{o}G_{Al:Mn:Al}$	-16 418.98	5.568
		${}^{o}G_{Al:Mn:Mn}$	-26 001.95	5.944
		${}^{o}L$	-12 133.60	3.981
Beta (CUB)	SSM	${}^{o}L$	-1 10 959.68	41.873
		${}^{1}L$	-21 756.80	25.90

*CEF- Compound Energy Formalism, SSM- Substitutional Solution Model, ST- Stoichiometric compound

Table 4.2 The optimized parameters of the stable phases in the Mn-Zn system

Description of the pure element in metastable phases [1]	Phase	Parameters	**C** (J/mol atom)	**D** (J/mol atom K)
Zn (CBCC) = Zn (HCP) + 3347.20 J/mol Zn (CUB) = Zn (HCP) + 1882.80 J/mol	Liquid	${}^{o}L$	-3 242.60	1.381
	Alpha (CBCC)	-	-	-
	Beta (CUB)	${}^{o}L$	-30 877.92	71.672
		${}^{1}L$	47 279.20	84.349
		${}^{2}L$	75 730.40	9.623
	Gamma (FCC)	${}^{o}L$	-13 765.36	5.816
		${}^{1}L$	11 673.36	-6.569
	Delta (BCC)	${}^{o}L$	-9 259.20	-
		${}^{1}L$	13 363.70	-11.129
		${}^{2}L$	9 330.32	-7.406
	Zn (HCP)	${}^{o}L$	4 602.40	-
	Epsilon (HCP)	${}^{o}L$	-702.49	-1.975
		${}^{1}L$	-502.1	1.151
		${}^{2}L$	-10 167.12	8.870
	Zn_8Mn_5	${}^{o}G_{Mn:Zn}$	7 576.26	-4.377
		${}^{o}G_{Zn:Zn}$	74.03	-
		${}^{o}L$	-15 342.41	13.839
	$Zn_{13}Mn$	$\Delta G_{Zn_{13}Mn}$	-1 535.71	-0.449
	Zn_9Mn	ΔG_{Zn_9Mn}	-1 750.00	-1.107
	Zn_3Mn	ΔG_{Zn_3Mn}	-3 750.00	-0.784
	ZnMn	ΔG_{ZnMn}	-7 000.00	5.34

[1] The parameters for pure Zn in metastable CBCC and CUB phases are optimized in this work because they are unavailable in the literature.

Table 4.3 The optimized parameters of the stable binary phases in Mg-Mn system

System	Phase	Parameters	**C** (J/mol atom)	**D** (J/mol atom K)
Mg-Mn	Liquid	${}^{o}L$	22 973.44	0.808
		${}^{1}L$	-11 995.18	0.0
	Mg (HCP)	${}^{o}L$	46 643.23	-8.828
		${}^{1}L$	-3 322.10	0.0
	Gamma (FCC)	${}^{o}L$	83 680.00	0.0
	Delta (BCC)	${}^{o}L$	83 680.00	0.0

Table 4.4 The optimized parameters for the stable ternary phases in Mg-Al-Mn system

System	Phase	Parameters	**C** (J/mol atom)	**D** (J/mol atom K)
Mg-Al-Mn	Liquid	${}^{o}L_{Al,Mn:Mg}$	15 480.80	0.0
	$Mg_3Al_{18}Mn_2$ (T)	$\Delta G_{Mg_3Al_{18}Mn_2}$	-8 695.65	.006

With the optimized parameters for each of the phases in the binary and ternary systems, all the calculated phase equilibria and thermodynamic properties in relation to the reliable experimental results from the literature for the Al-Mn, Mg-Mn, Mn-Zn, Mg-Al-Mn and Mg-Mn-Zn systems have been discussed in detail in the subsequent sections.

4.2 Al-Mn System

The calculated Al-Mn phase diagram with their stable phases is shown in figure 4.1. The corresponding calculated invariant reactions and the compositions of the respective phases are given in table 4.5.

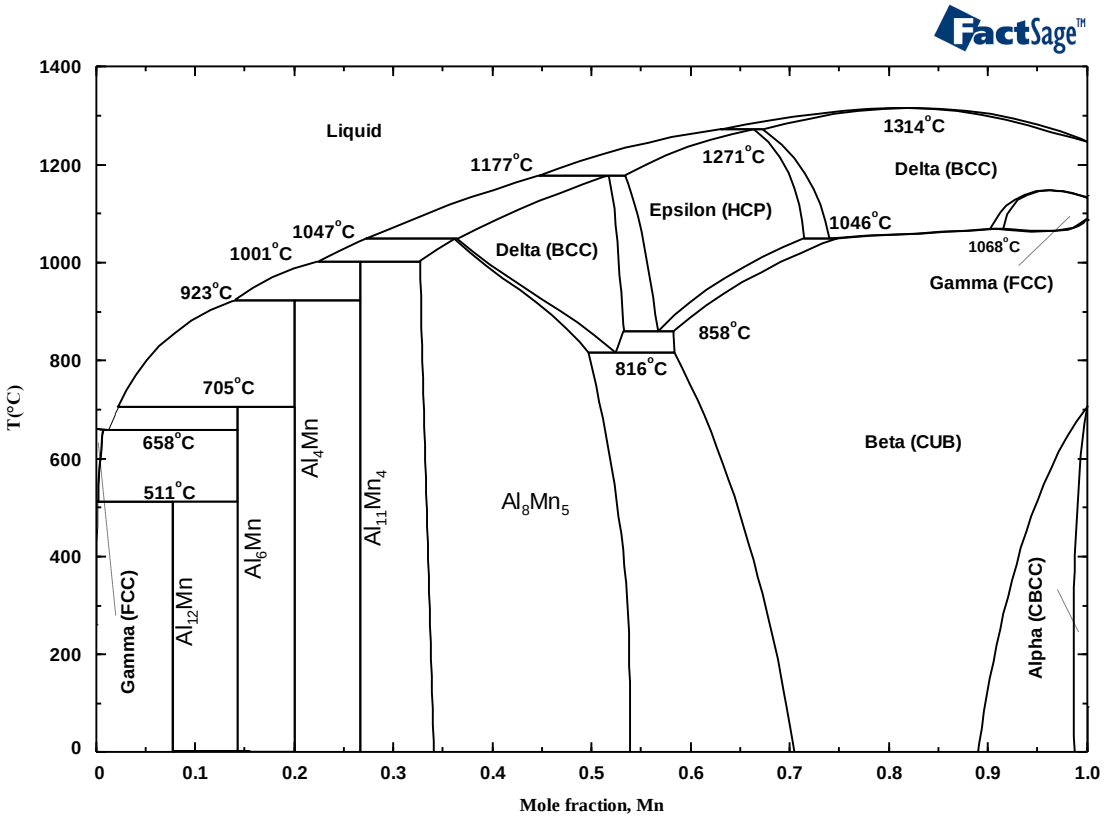

Fig 4.1 Calculated Al-Mn phase diagram

Table 4.5 Calculated invariant points in the Al-Mn system compared with the experimental data of [9,24,118-121]

Reaction	Type	Temp. °C	Composition at % Mn			Reference
FCC + $Al_6Mn \Leftrightarrow Al_{12}Mn$	Peritectoid	511	0.2	14.3	7.7	This work
		504 - 521	-	-	-	[119]
L $\Leftrightarrow$ Gamma (FCC) + Al_6Mn	Eutectic	658	1.0	0.6	14.3	This work
		658	0.99	-	-	[120]
L + $Al_4Mn \Leftrightarrow Al_6Mn$	Peritectic	705	2.4	20.0	14.3	This work
		705	-	19.00	-	[121]
L + $Al_{11}Mn_4 \Leftrightarrow Al_4Mn$	Peritectic	923	14.4	26.7	20.0	This work
		923	15.00	24.20	21.00	[121]
L + $Al_8Mn_5 \Leftrightarrow Al_{11}Mn_4$	Peritectic	1001	22.6	31.5	26.7	This work
		1002	22.30	30.00	28.00	[121]

Table 4.5 Calculated invariant points in the Al-Mn system compared with the experimental data (Contd.)

Reaction	Type	Temp. °C	Composition at % Mn			Reference
L + Delta (BCC) ⇔ Epsilon (HCP)	Peritectic	1271	65.5	68.7	67.9	This work
		1260	-	-	-	[121]
		1280	-	-	-	[9]
		1256	-	-	-	[24]
HCP ⇔ Delta (BCC) + Beta (CUB)	Eutectoid	858	56.7	53.2	58.3	This work
		870	-	-	-	[121]
		870	55.00	50.05	60.00	[118]
		870	58.00	53.50	60.60	[9]
		857	-	-	-	[24]
L + Delta (BCC) ⇔ Al_8Mn_5	Peritectic	1047	27.5	36.4	36.1	This work
		1048	28.30	34.50	33.60	[121]
L + Epsilon (HCP) ⇔ Delta (BCC)	Peritectic	1177	44.8	53.4	51.8	This work
		1160	-	-	-	[120]
		1190	-	-	-	[24]
Delta (BCC) ⇔ Al_8Mn_5 + Beta (CUB)	Eutectoid	816	52.3	49.8	58.4	This work
		840	49.50	47.00	59.50	[121]
		817	-	-	-	[24]
Delta (BCC) + Gamma (FCC) ⇔ Beta (CUB)	Peritectoid	1068	89.8	92.5	91.0	This work
			-	-	-	-
Delta (BCC) ⇔ Epsilon (HCP) + Beta (CUB)	Eutectoid	1046	71.4	72.1	76.0	This work
		1040	74.50	71.50	75.50	[9]
		903	-	-	-	[24]
L ⇔ Delta (BCC)	Congruent	1314	82.8	82.8		This work
			-	-	-	-
Beta (CUB) ⇔ Gamma (FCC)	Congruent	1061	95.7	95.7		This work
			-	-	-	-

The calculated Al-Mn phase diagram has an overall good agreement with the experimental results from the literature as shown in figures 4.2 through 4.4. The calculated solid solubility of Mn in Al has been compared with the solubility

measurements of [15-17,19,25-28] and the calculation of the most recent work of Shukla and Pelton [30] on this system as shown in figure 4.2. The current calculation almost reproduces the EPMA results of Minamino et al. [26] while showing a good agreement with the mutually consistent data. The calculation of [30] is also acceptable considering the uncertainty of the experimental results although the agreement with a particular set of data is not evident as can be seen in figure 4.2. The current calculation is not consistent with the measured solubility of Drits et al. [15]. It is worth noting that these measurements [15] are not consistent with the other experimental results which may be due to the possible iron contamination of their samples as pointed out in [14].

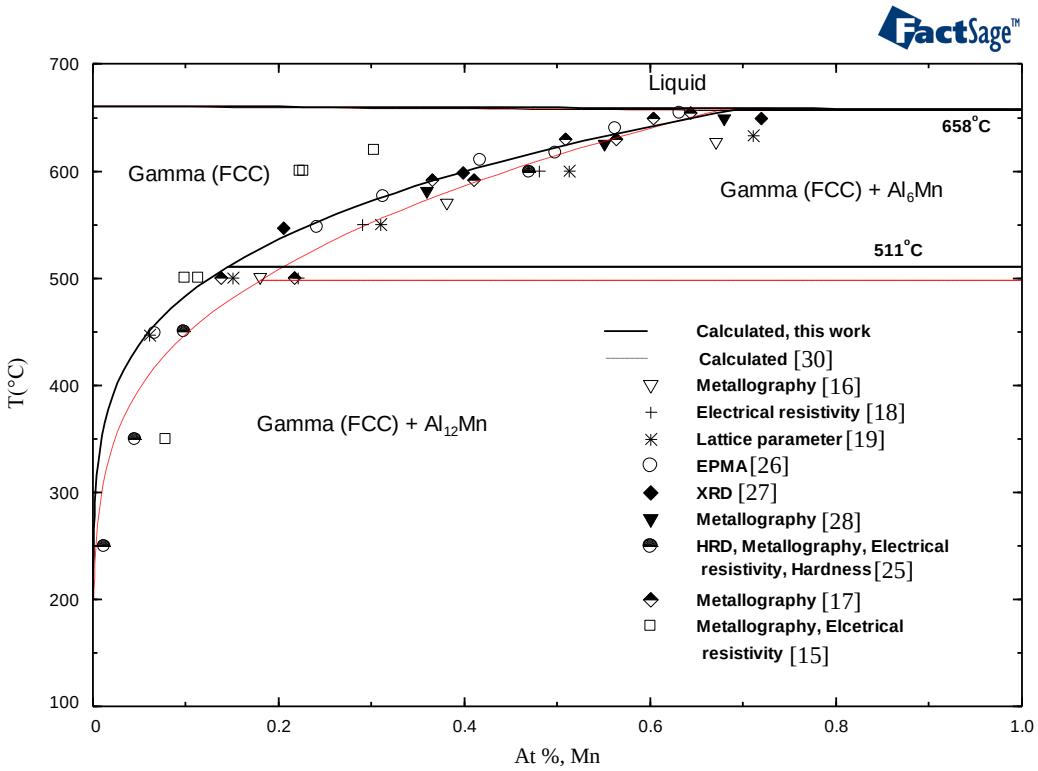

Fig 4.2 Calculated solubility of Mn in Al compared with the data measured by [15-19,25-28] and the calculation of [30]

The calculated Al-rich portion (< 45 at %, Mn) is shown in figure 4.3. Only the thermal analyses heating data rather than the cooling data of [16,29,120-123] have been compared here in order to avoid the inconsistencies that might result from possible undercooling effect. The reliable data in this region are well reproduced in the calculation.

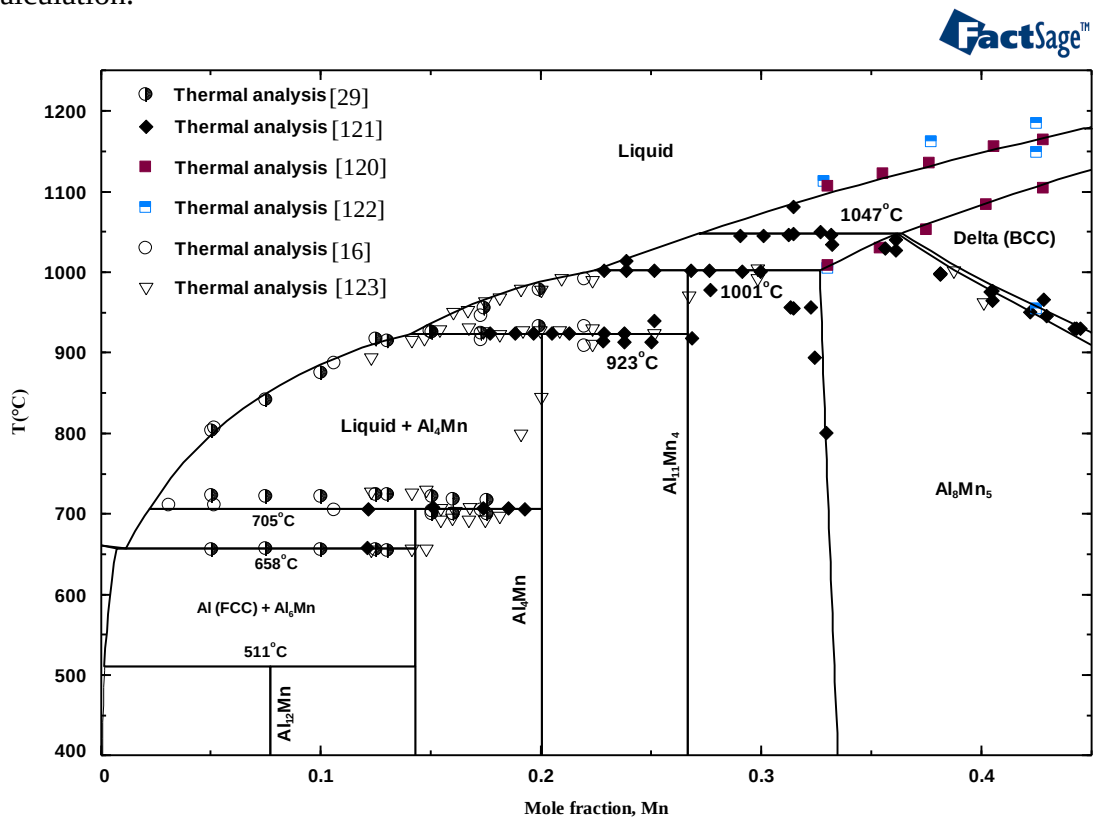

Fig 4.3. Calculated Al-rich part of the Al-Mn phase diagram with the experimental results of [16,29,120-123]

It is to be noted here that the near stoichiometric phase μ-Al_4Mn, of which, Okamoto [23] questioned the existence because of its proximity to the other stoichiometric λ-Al_4Mn phase, has been ignored in the current work. Also, the other stable phase which shows a narrow homogeneity range and often termed as the high temperature modification of the $Al_{11}Mn_4$, has been modeled as stoichiometric compound

for the sake of simplicity. However, this simplification does not lead to a significant error in the higher order systems as discussed by Jansson [22]. Also, the possible existence of order-disorder transition in the intermediate Delta (BCC) phase in the middle of the phase diagram as stated by Liu et al. [10] was not modeled in the current work due to lack of experimental evidence.

In figure 4.4, a portion of the calculated phase diagram is compared with the accepted experimental results of [9,24,118,120-123] and [9,24,117,119-121] and the calculation of [30].

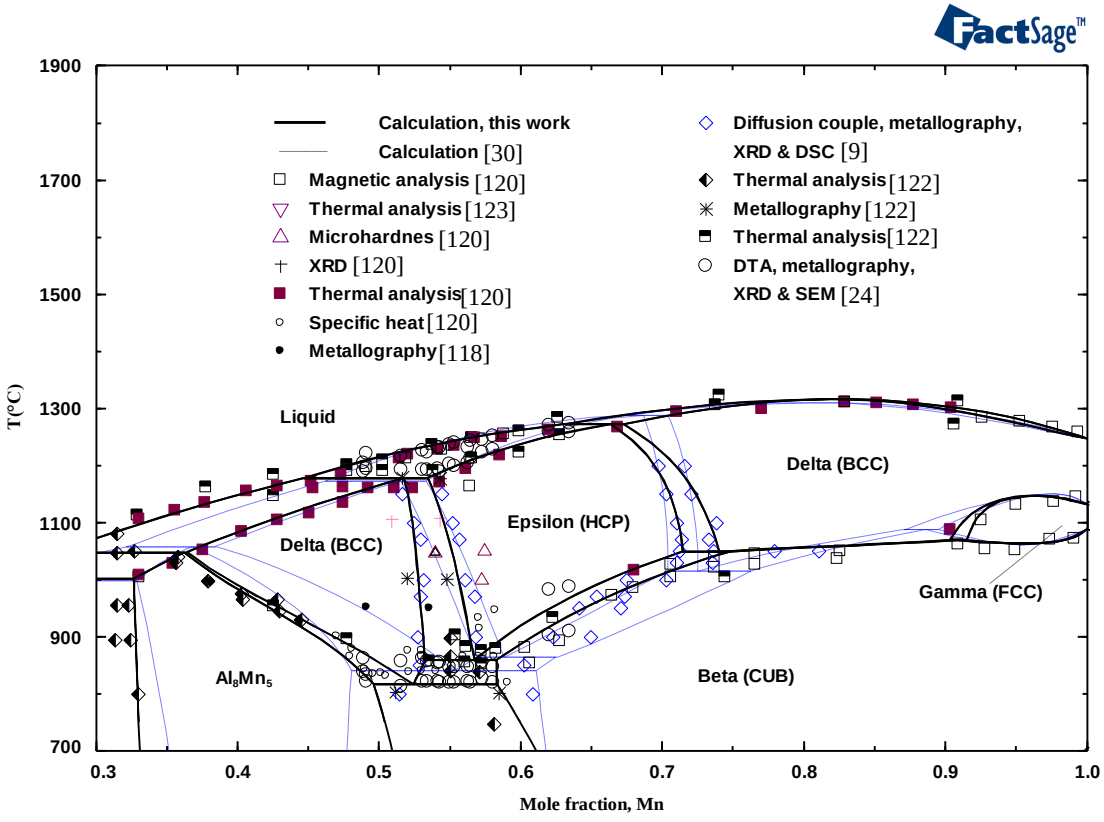

Fig 4.4 Calculated Mn-rich portion of the Al-Mn phase diagram compared with the experimental results of [9,24,118,120-123] and calculation of [30]

The current calculation shows a better agreement with the experimetnal data compared with the calculation of [30]. Also, the current calculation is consistent with the observation of Okamoto [23] who suggested a smooth continuous liquidus curve between the terminal Delta (BCC) and intermediate Delta (BCC) solid solution phase throughout the Epsilon (HCP) phase as mentioned in [10]. The other available calculations [10,22] are also consistent with this observation while the calculated liquidus lines of [30] did not maintain this condition.

Figure 4.5 shows that the enthalpy of mixing of the Al-Mn liquid measured by Esin et al. [31] showing a large negative value with a minimum around 45 at % Mn has been reproduced satisfactorily in the current calculation.

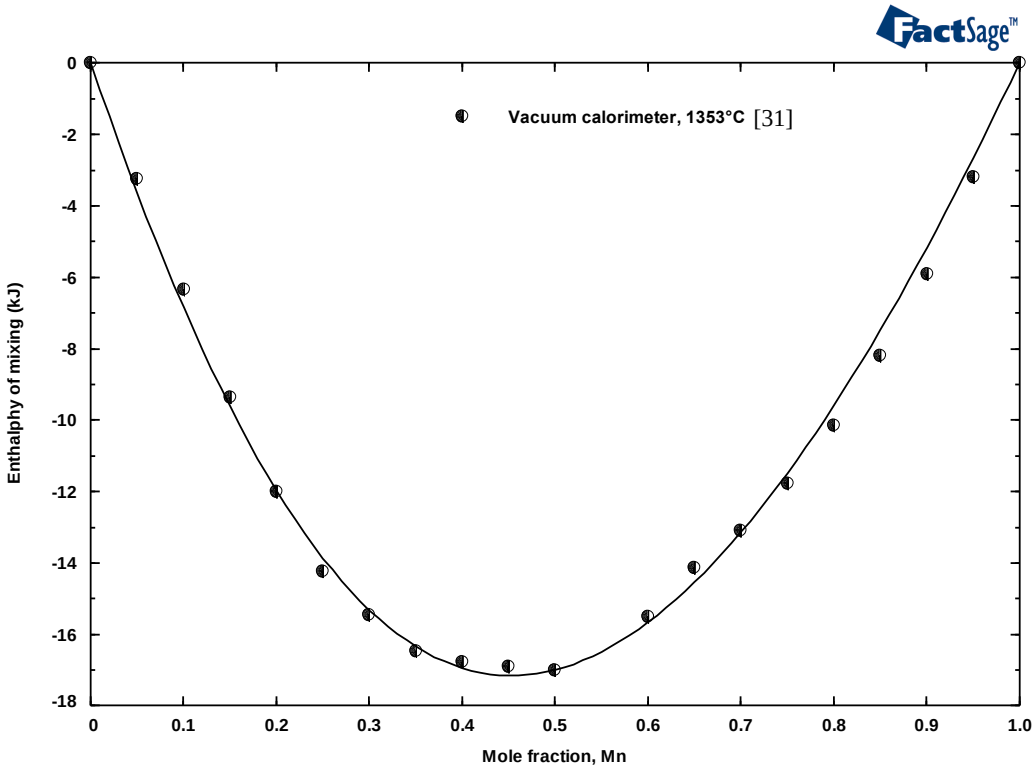

Fig 4.5 Calculated enthalpy of mixing of liquid Al-Mn alloy at 1353°C compared with the measured values from [31]

The activities of the components in the Al-Mn melt measured by Batalin et al. [32] and Chastel et al. [33] have been compared with the current calculation as well as the calculation of [30] in figure 4.6. The current calculation is consistent with both the experimental data while favoring the more recent data of Chastel et al. [33] who used Knudsen effusion cell for their measurements. The calculation of [30] is not consistent with these data as can be seen in figure 4.6.

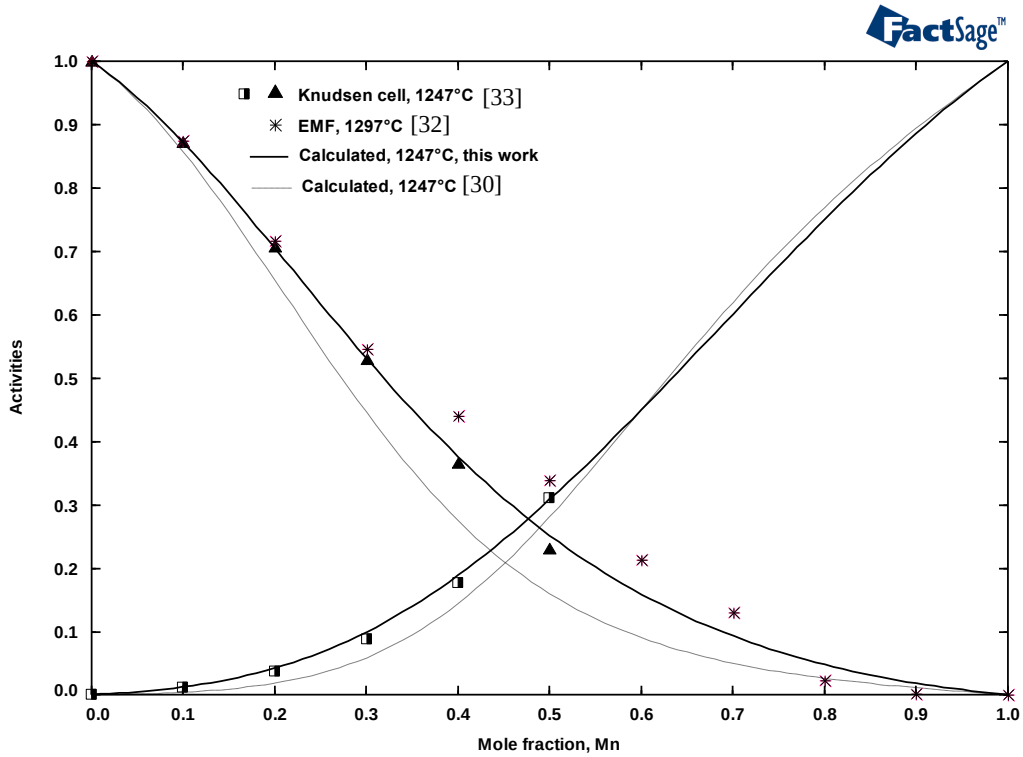

Fig 4.6 Calculated activities of Al and Mn in the Al-Mn liquid alloys compared with the measured values from [32,33] and calculation of [30]

In figure 4.7, the experimental enthalpy of formation of some of the solid Al-Mn alloys and the calculated results of [30] has been compared with the current calculation. The current calculation reproduces the experimental data within the experimental error limits for all the composition of Al-Mn alloy except near the middle composition of the

phase diagram. At 50 at% Mn, the current calculation predicts lower enthalpy of formation than the value measured by Kubaschewski and Heymer [34]. It should also be noted that [34] reported two different values of formation enthalpy for the same composition at 50 at% Mn which may be an indication of significant uncertainty associated with the data at this composition. Nevertheless, the current results are generally closer to the experimental values than those of [30].

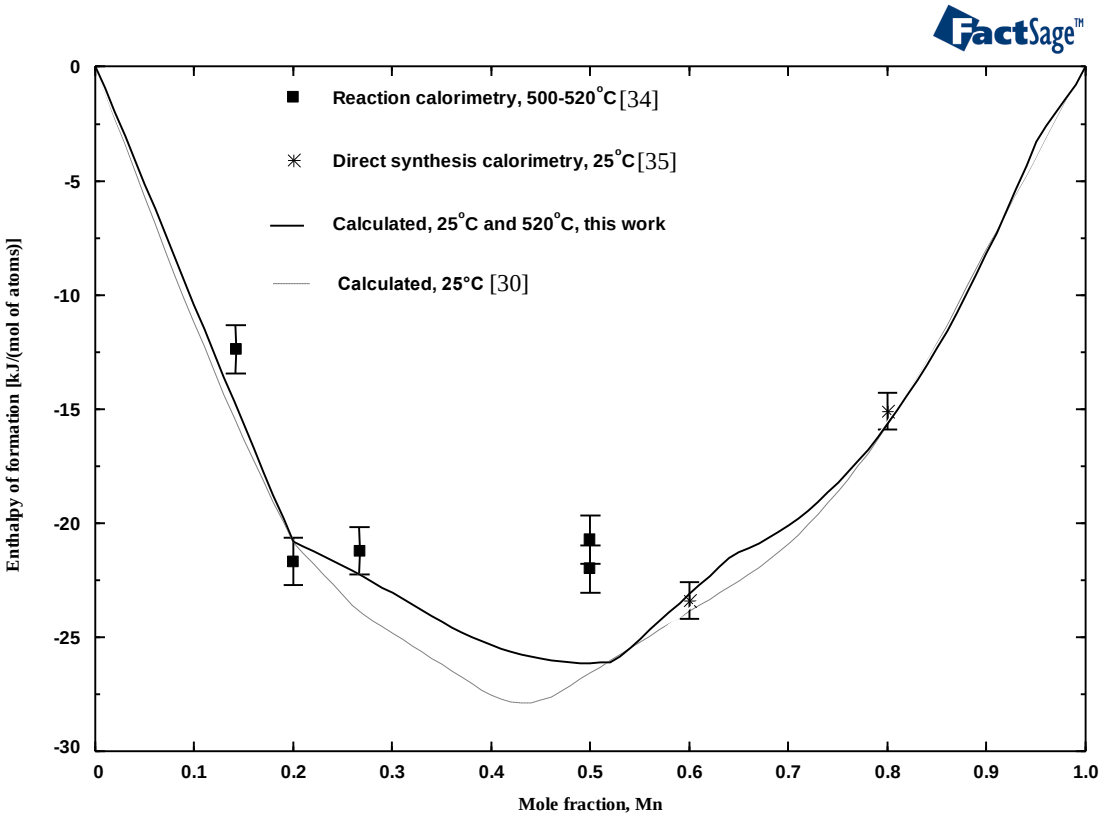

Fig 4.7 Calculated enthalpy of formation of some solid Al-Mn alloys compared with the measured values from [34,35] and the calculation of [30]

In figure 4.8, the calculated log activity versus composition has been compared with the measured values of Kematick and Myers [36]. They [36] linked the data points of the Mn activities and found that their measurement of the activity of Mn is consistent

with the assessed Al-Mn phase diagram of McAlister et al. [14]. The current calculation reasonably agrees with the measurements of Mn activities as shown in figure 4.8. In the most recent assessments of the Al-Mn system, Du et al. [29] and Shukla and Pelton [30] did not use the data of [36] claiming it to be inconsistent with the other data of the system.

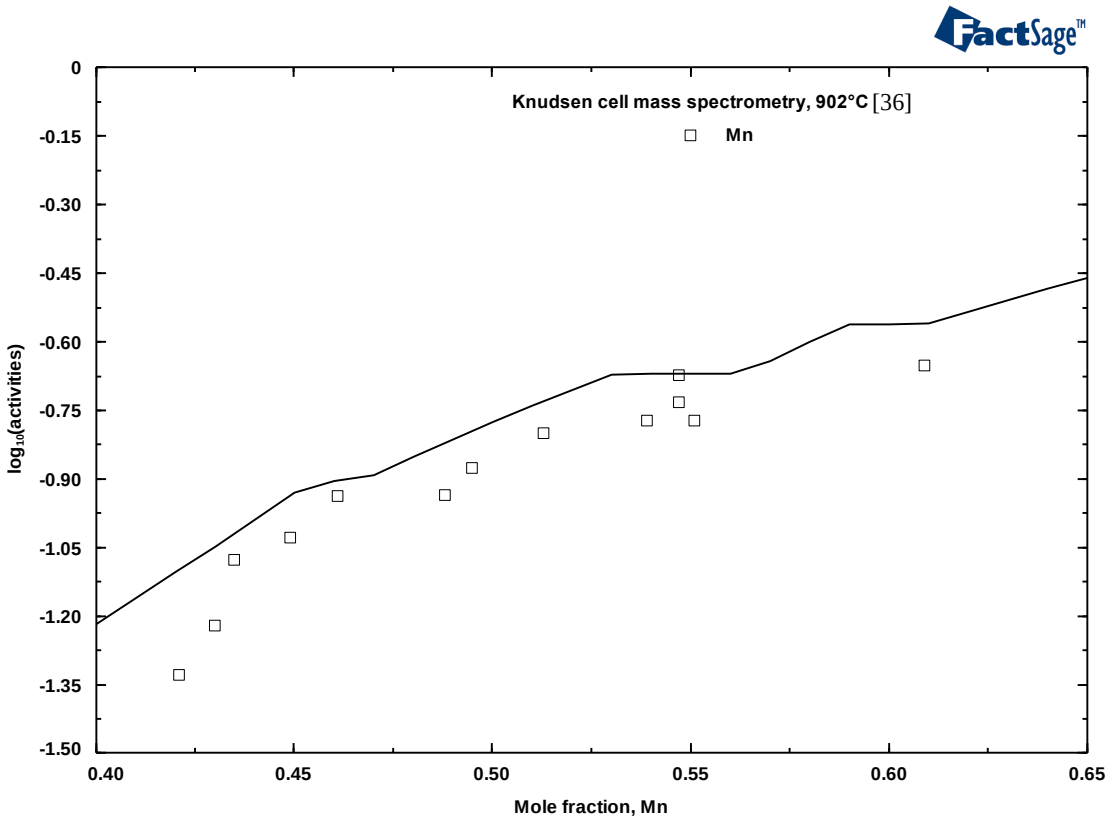

Fig 4.8 Comparison of the calculated log activity vs composition with the measured values from [36]

In table 4.6, the number of parameters used for optimizing the Al-Mn system is compared between the current work and the work of Shukla and Pelton [30] who also used the MQC model for the liquid phase. The number of model parameters and coefficients used for the different phases in this work is either less than or equal to that of

the work of [30]. Further, the agreements with the experimental results are generally better in the current work than in the work of [30].

Table 4.6 Comparison of the number of model parameters used for optimizing the Al-Mn system between this work and the work of [30]

Phase	Model * used	No. of Parameters	No. of coefficients	Reference
Liquid	MQC	2	4	This work
		3	6	[30]
Alpha (CBCC)	SSM	2	3	This work
		2	3	[30]
Beta (CUB)	SSM	2	4	This work
		2	4	[30]
Gamma (FCC)	SSM	1	2	This work
		2	4	[30]
Delta (BCC)	SSM	2	4	This work
		2	4	[30]
Epsilon (HCP)	SSM	3	6	This work
		3	6	[30]
Al_8Mn_5	CEF, three sublattices	1	2	This work
		2	4	[30]

*CEF- Compound Energy Formalism, SSM- Substitutional Solution Model

4.3 Mg-Mn System

The calculated Mg-rich portion of the Mg-Mn phase diagram has been compared with the experimental data from [40,42,44-49] as shown in figure 4.9. The calculated solubility of Mn in Mg favors the data of Drits et al. [49], Grogan et al. [42] and Petrov et al. [47] which are self-consistent but deviate from the data of Schmid and Siebel [40] who measured higher Mn content in the solution. Similarly, the liquidus data of Petrov et al.

[47] who measured higher liquidus temperature is favored in the calculation as shown in figure 4.9. This is because the higher liquidus temperatures were expected considering the sources of error in the dip sampling technique which was used to measure the liquidus curve in the Mg-Mn system.

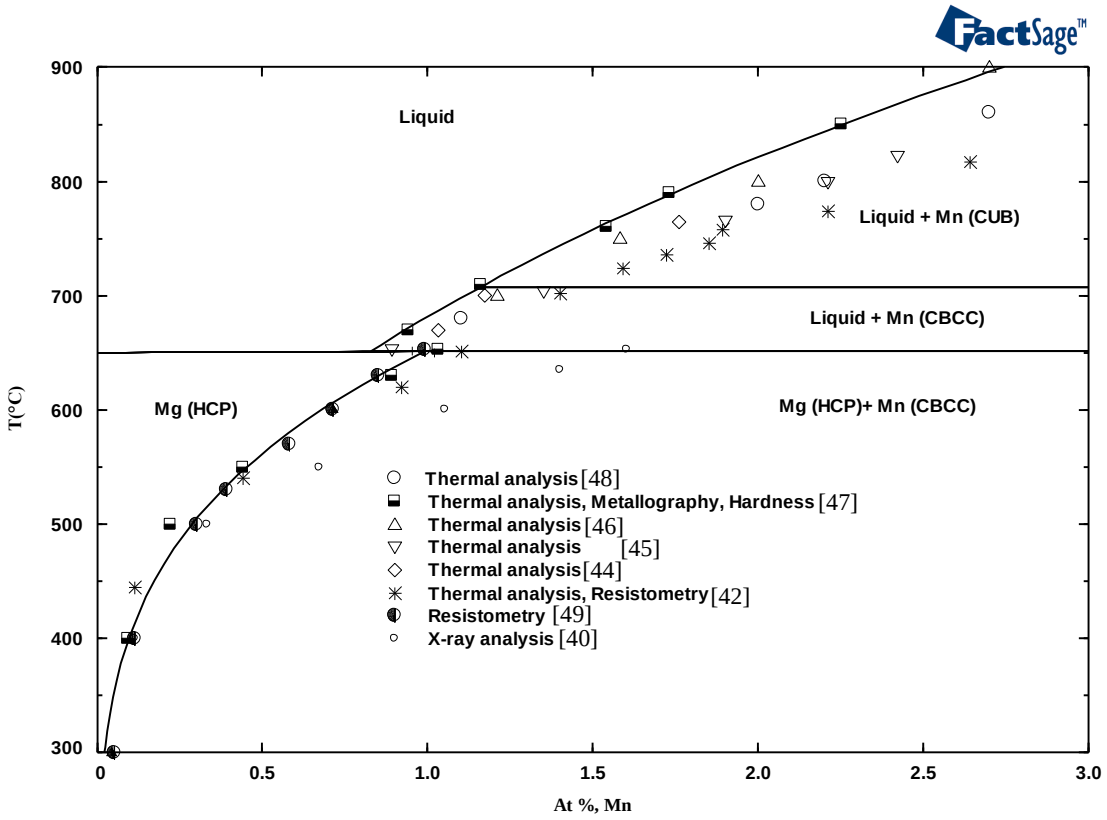

Fig 4.9 Comparison of the calculated Mg-rich portion of the Mg-Mn phase diagram with the data from [40,42,44-49]

In figure 4.10, the calculated Mg-Mn phase diagram has been compared with the experimental phase diagram data of Gröbner et al. [57] who used DTA, SEM and EDS. They [57] measured the binary monotectic temperature whose lower limit was reported to be around 1200°C. The possible underestimation of temperature due to the reaction of the crucible material with the liquid Mn was reported to be the reason for depicting the

measured monotectic temperature as the lower limit. The current model calculates the monotectic reaction temperature as 1206°C which is in agreement with the observation of [57] as can be seen in figure 4.10.

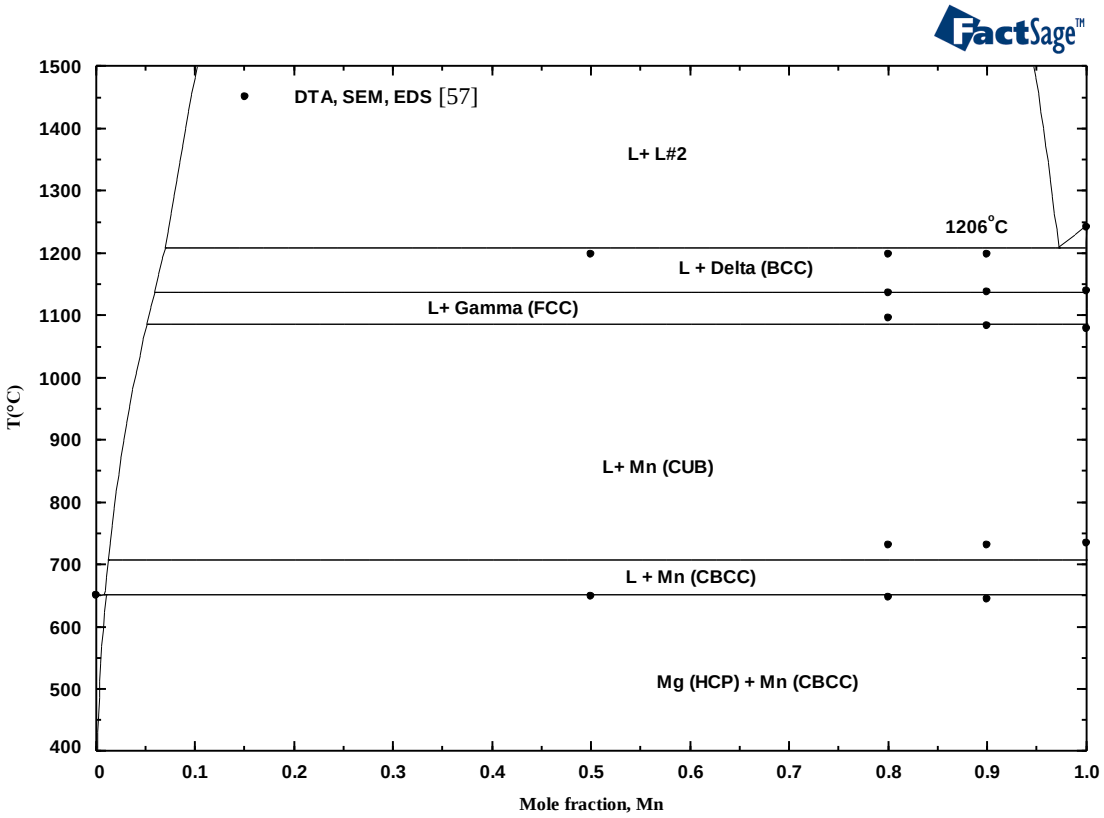

Fig 4.10 Comparison of the calculated Mg-Mn phase diagram with the experimental values from [57]

In table 4.7, some of the calculated thermodynamic properties of the liquid phase in similar binary systems which show extended miscibility gap in the liquid have been compared. The values of the thermodynamic quantities are comparable with the values of the similar systems. Further, the calculated critical temperature of the miscibility gap near the equiatomic composition is found to be 3056K. This value is also comparable with the model of [57] which calculates it at 3475K. The percentage deviation of the current value

of the critical temperature, from the estimated value using Predel's [124] empirical equation, falls within the range of the percentage deviation of other similar systems as shown in the last column of table 4.7. The author finds it more reasonable to evaluate the current model on the basis of such thermodynamic considerations rather than to use one experimental information in a specific higher order system to validate the reliability of the calculation in a lower order system as performed in [58]. No relevant experimental information on any other ternary systems involving Mg-Mn as a constituent system are available, except the result of Antion [59], to support the conclusion of [58] that the critical temperature of the Mg-Mn miscibility gap should be far less than that calculated in [57]. The present calculation relies on the comparison of the thermodynamic quantities with other similar systems which gives a reasonable basis for the reliability of the current model in the absence of relevant experimental information on the Mg-Mn system.

Table 4.7 Comparison of thermodynamic properties of liquid binary alloys at equiatomic composition exhibiting extended miscibility gap in liquid [125]

Alloys	Temperature (K)	G_M^{xs}/RT [125]	H_M/RT [125]	S_M^{xs}/R [125]	Estimated $Tcr^1 = 2H_m/(R + 2 S_M^{xs})$ (K), [124], p	T_{cr} (K) Assessed, q	% deviation $\frac{\lvert p-q \rvert}{q} * 100$
Al-In	1150	0.540	0.490	-0.050	1251	1112	12.5
Al-Pb	1700	0.527	0.847	0.320	1755	1700	3.2
Bi-Zn	880	0.360	0.600	0.240	713	864	17.5
Cd-Ga	695	0.485	0.484	-0.001	337	560	39.8
Mg-Mn*	3450*	0.427*	0.332*	-0.095*	3056	3688*	17.1

* Calculation using the current model

[1]: Critical temperature of liquid miscibility gap

4.4 Mn-Zn System

The current modeling of the Mn-Zn binary system can be considered as a significant improvement of the Miettinen's [96] work. The optimized system provides better agreement with the representative experimental data and includes some of the low temperature phases which were excluded in Miettinen's [96] work. The optimized phase diagram is shown in figure 4.11 together with the experimental data of [89,93] recommended by Okamoto and Tanner [60].

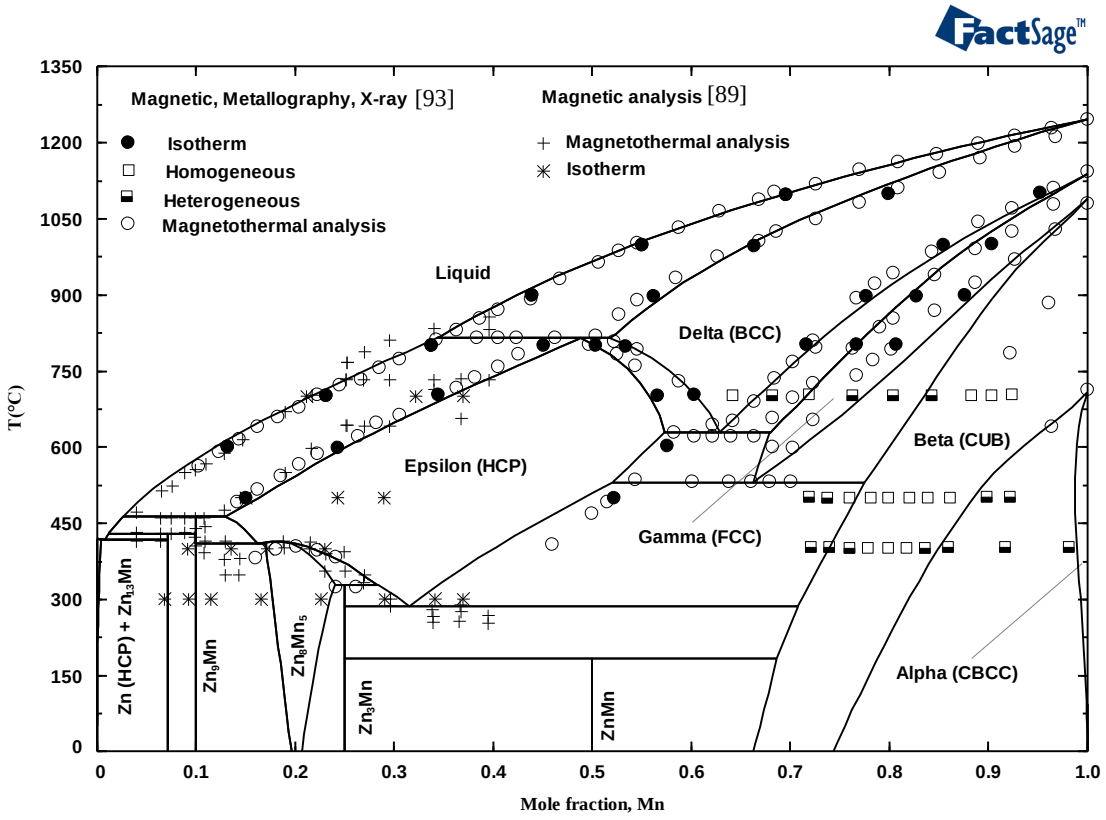

Fig 4.11 Calculated Mn-Zn phase diagram compared with the experimental results of [89,93]

The calculated phase diagram throughout the entire composition and temperature range shown in the figure agrees well with the accepted experimental phase diagram data.

The calculated phase boundary between Beta (CUB)/[Alpha (CBCC) + Beta (CUB)] in the Mn-rich part of the system with the current model shows better agreement with the magnetothermal, XRD and metallographic observations of Romer et al. [93] than the description of Miettinen [96] as can be seen comparing the figures 4.11 and 2.6.

In table 4.8, the calculated invariant reactions in the Mn-Zn binary system are compared with the experimental data of [61,62,64,65,70,71,74,81,89,93].

Table 4.8 Calculated invariant points in the Mn-Zn system compared with the experimental data

Reaction	Type of reaction	Temp. °C	Composition at % Zn			Reference
L ⇔ Delta (BCC) + Epsilon (HCP)	Peritectic	815	65.5	48.1	51.1	This work
		815	65.0	50.0	53.0	[93]
		835	62.0	47.0	50.0	[70]
Delta (BCC) ⇔ Gamma (FCC) + Epsilon (HCP)	Eutectoid	627	37.2	32.0	42.8	This work
		620	38.0	34.0	42.0	[93]
		650	40.0	35.0	-	[74]
FCC ⇔ Beta (CUB) + Epsilon (HCP)	Eutectoid	530	33.8	22.4	47.7	This work
		530	31.0	25.0	46.0	[93]
		554	35.0	18.0	-	[74]
Epsilon (HCP) ⇔ Beta (CUB) + Zn_3Mn	Eutectoid	282	68.6	29.3	75.0	This work
Beta (CUB) + Zn_3Mn ⇔ ZnMn	Peritectoid	180	31.44	75.00	50.00	This work
		180	47.00	70.00	50.00	[81]
Epsilon (HCP) + Zn_8Mn_5 ⇔ Zn_3Mn	Peritectoid	325	71.67	76.00	75.00	This work
		325	72.00	77.00	74.50	[70]
Epsilon (HCP) ⇔ Zn_8Mn_5	Congruent transition	413	81.56	81.56	-	This work
		400	80.80	80.80	-	[70]
		420	-	-	-	[89]
Epsilon (HCP) ⇔ Zn_9Mn + Zn_8Mn_5	Eutectoid	408	83.9	90.00	83.11	This work

Table 4.8 Calculated invariant points in the Mn-Zn system compared with the experimental data (Contd.')

Reaction	Type	Temp. °C	Composition at % Zn			Reference
L + Epsilon (HCP) $\Leftrightarrow$ Zn_9Mn	Peritectic	462	97.40	87.00	90.00	This work
		462	96.30	88.60	90.00	[70]
		462	-	88.5	90.00	[89]
L + Zn_9Mn $\Leftrightarrow$ $Zn_{13}Mn$	Peritectic	428	98.70	90.00	92.86	This work
		428	98.10	90.60	92.70	[70]
		430	-	90.50	92.00	[89]
L $\Leftrightarrow$ $Zn_{13}Mn$ + Zn (HCP)	Eutectic	416.9	99.23	92.86	99.60	This work
		418	99.3	87.5	100	[61]
		400	96	80	98	[62]
		416	99	87.2	100	[62]
		419	98.9	87.5	99.5	[64]
		414	99.5	90	100	[65]
		416	98.6	92.9	99.4	[70]
		417.25	-	-	-	[71]
		416	-	-	-	[89]

It is seen from the above table that most of the experimentally observed invariant reactions are reasonably reproduced. The most ambiguous portion of the phase diagram, as mentioned by Okamoto and Tanner [60] is the epsilon (HCP) phase field. Due to the lack of confirming data this phase is modeled as only one wide field in the current work instead of possible existence of three separate phase fields as suggested by [60]. For this reason, some of the speculated invariant reactions invlolving different allotropies of epsilon (HCP) phase were not taken into consideration in the current work. The deviations of compositions of some of the invariant reactions shown in table 4.8 can be explained by the fact that some of the solid solutions which show narrow homogeneity range have been modeled as stoichiometric in this work. Also, it should be pointed out

that the possible order-disorder transition of the Delta (BCC) phase has not been considered in the present modeling as no experimental evidence could be found in the literature.

The calculated thermodynamic properties have been compared with the experimental measurments in figures 4.12 through 4.14. The activity of Zn in the Mn-Zn liquid measured by Baker et al. [95] is reproduced by the current model as shown in figure 4.12. In figure 4.13, the activity of Zn in Mn rich alloy measured by Dimov et al. [126] at 1300°C agrees well with the current calculation. In figure 4.14, the calculated activity of Zn in solid Mn-Zn alloy at 420°C also shows a good agreement with the measured value of Anantatmula [94].

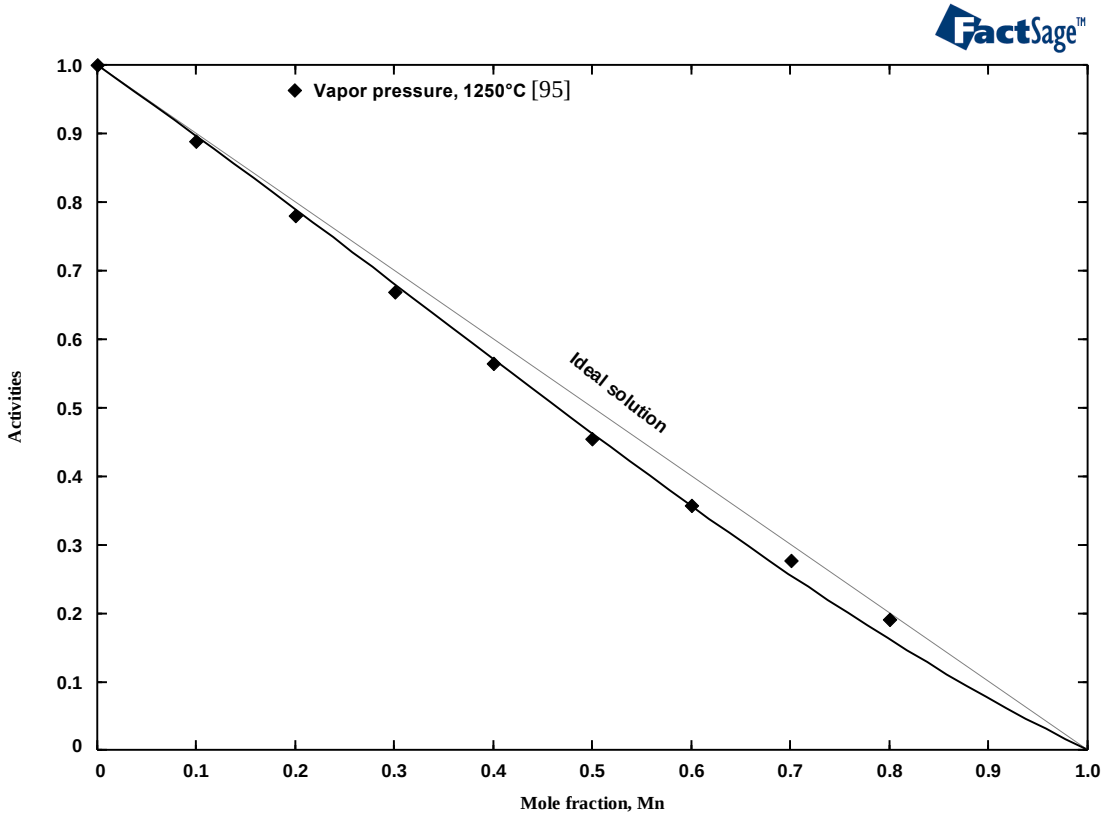

Fig 4.12 Calculated activity of Zn in liquid Mn-Zn alloys at 1250°C compared with the measured values of [95]

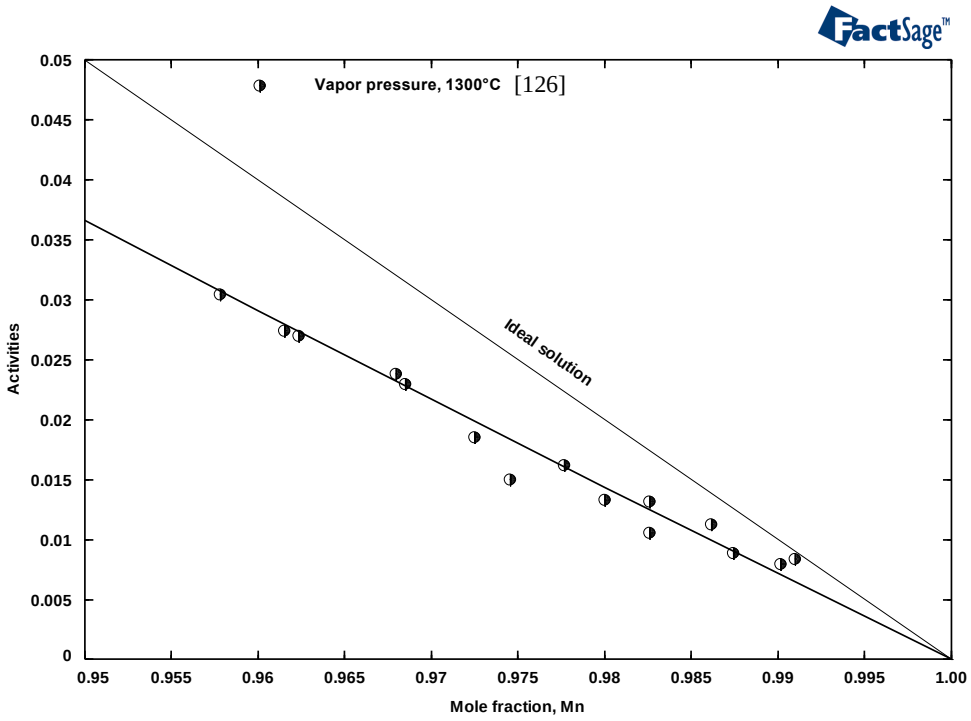

Fig 4.13. Calculated activity of Zn in liquid Mn-Zn alloys at 1300°C compared with the measured values of [126]

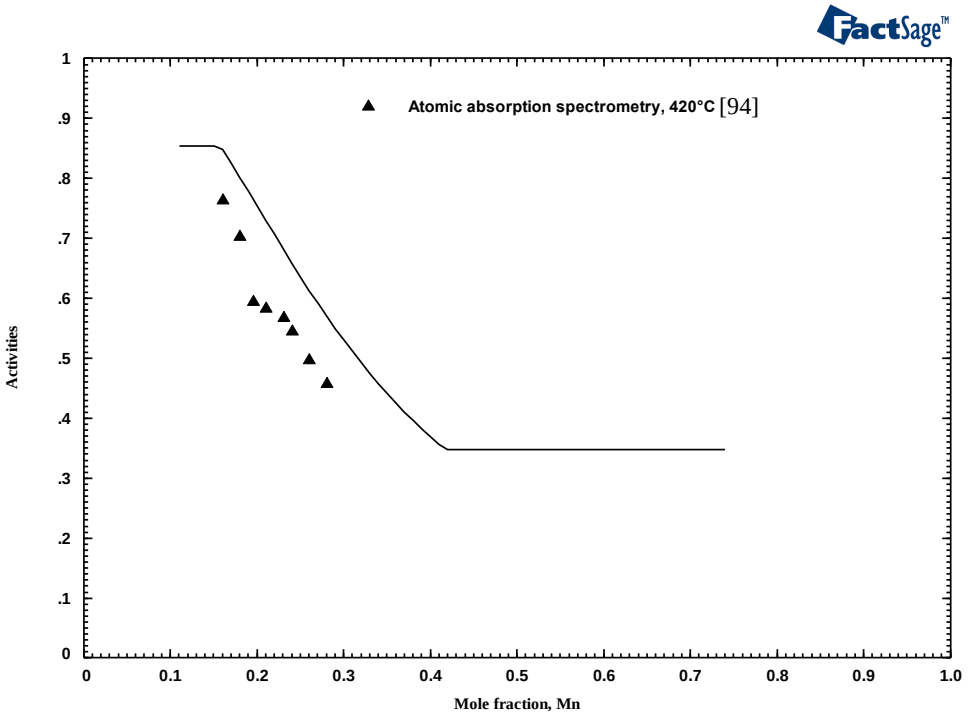

Fig 4.14. Calculated activity of Zn in solid Mn-Zn alloys at 420°C compared with the measured values of [94].

The experimental data presented in figures 4.12 to 4.14 are the only experimental thermodynamic properties that could be found in the literature for the Mn-Zn binary system and the current model is capable of reproducing them reasonably well. Thus, a single set of parameters for each of the stable phases in the Mn-Zn system can handle all of the phase diagram as well as the thermodynamic data.

The optimized parameters for the binary systems are combined to extrapolate to the ternary Mg-Al-Mn and Mg-Mn-Zn systems. A good description of the Mg-Al-Mn ternary system has been found by the Kohler [127] symmetric extrapolation scheme with only one ternary interaction parameter for the liquid phase. The same extrapolation method is used for the Mg-Mn-Zn system as well but no ternary interaction parameters are used. The ternary descriptions and the results are discussed in the following sections.

4.5 Mg-Al-Mn System

A series of calculations has been performed for the ternary Mg-Al-Mn system with the constructed database and the outcome has been compared with the experimental results in figures 4.15 through 4.26. In figure 4.15, the liquidus projection for the entire composition range of the Mg-Al-Mn system has been calculated. The Mg-rich part of the liquidus projection has been zoomed and shown in figure 4.16 with comparison to the available experimental data.

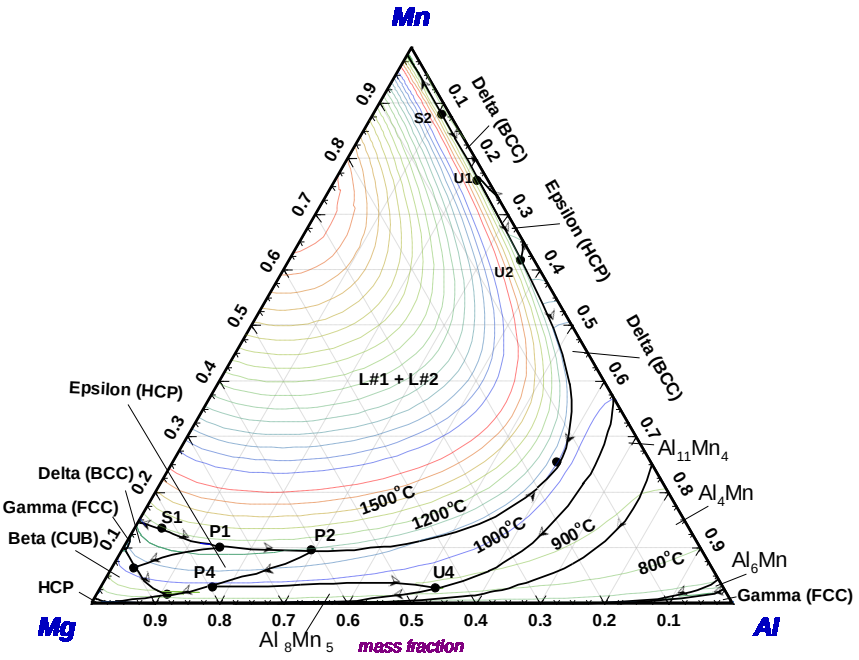

Fig 4.15. Calculated liquidus projection with arrows indicating the decreasing temperature (Dotted lines are isotherms)

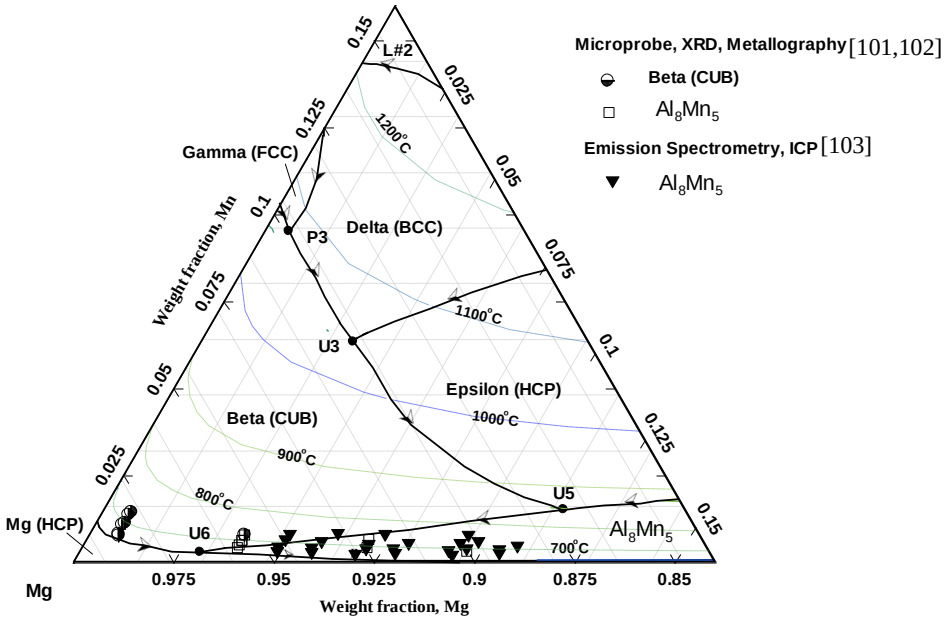

Fig 4.16. Liquidus projection in the Mg-rich corner of the Mg-Al-Mn system compared with the data of [101-103] (Dotted lines are isotherms.)

The liquidus projection in the Mg-rich corner of the Mg-Al-Mn system in figure 4.16 shows a reasonable consistency with the experimental data of Simensen et al. [101,102] and Thorvaldsen and Aliravci [103]. The invariant reactions in the ternary Mg-Al-Mn system have been calculated and are given in table 4.9. The type of reaction is also indicated in the table. Some degenerate invariant points also exist in the proximity of the Mg-Al edge which have not been shown in the table.

Table 4.9 Invariant points in Mg-Al-Mn system according to the current calculation

Reaction	T (K)	Type *	Composition (wt %)		
			Mn	Mg	Al
L#1 $\Leftrightarrow$ L#2 + Delta (BCC)	1573	S1	13.2	82.8	4.0
L#1 $\Leftrightarrow$ L#2 + Delta (BCC)	1573	S2	88.0	1.3	10.6
L#1 + Delta (BCC) $\Leftrightarrow$ L#2 + Epsilon (HCP)	1548	U1	75.9	1.6	22.5
L#1 + L#2 + Delta (BCC) $\Leftrightarrow$ Epsilon (HCP)	1523	P1	10.7	77.6	11.7
L#1 + Epsilon (HCP) $\Leftrightarrow$ L#2 + Delta (BCC)	1488	U2	59.4	2.3	38.3
L#1 + L#2 + Epsilon (HCP) $\Leftrightarrow$ Delta (BCC)	1438	P2	9.7	58.0	32.3
L#1 + FCC $\Leftrightarrow$ Beta (CUB) + Delta (BCC)	1343	P3	9.4	89.5	1.1
L#1 + Epsilon (HCP) + Delta (BCC) $\Leftrightarrow$ Al_8Mn_5	1248	P4	3.3	79.2	17.5
L#1 + Delta (BCC) $\Leftrightarrow$ Epsilon (HCP) + Beta (CUB)	1303	U3	6.6	90.3	3.1
L#1 + Delta (BCC) $\Leftrightarrow$ $Al_{11}Mn_4$ + Al_8Mn_5	1118	U4	2.8	44.9	52.3
L#1 + Epsilon (HCP) $\Leftrightarrow$ Beta (CUB) + Delta (BCC)	1118	U5	1.5	88.7	9.7
L#1 + Beta (CUB) $\Leftrightarrow$ Mg (HCP) + Al_8Mn_5	893	U6	0.3	96.7	2.9

* U: Transition type, P: Formation type. S: Saddle point.

Several isothermal sections, for which experimental information is available, have been calculated for the Mg-Al-Mn ternary system. The calculated isothermal section at 400°C, as shown in figure 4.17, agrees well with the data of Wakeman and Raynor [108] but does not agree with the data of Ohnishi et al. [110]. In figure 4.18, $Al_{12}Mn$ was found to exist at 400°C in addition to Al_6Mn. This is perhaps because $Al_{12}Mn$ was not known to exist in this system at the time of [109,110].

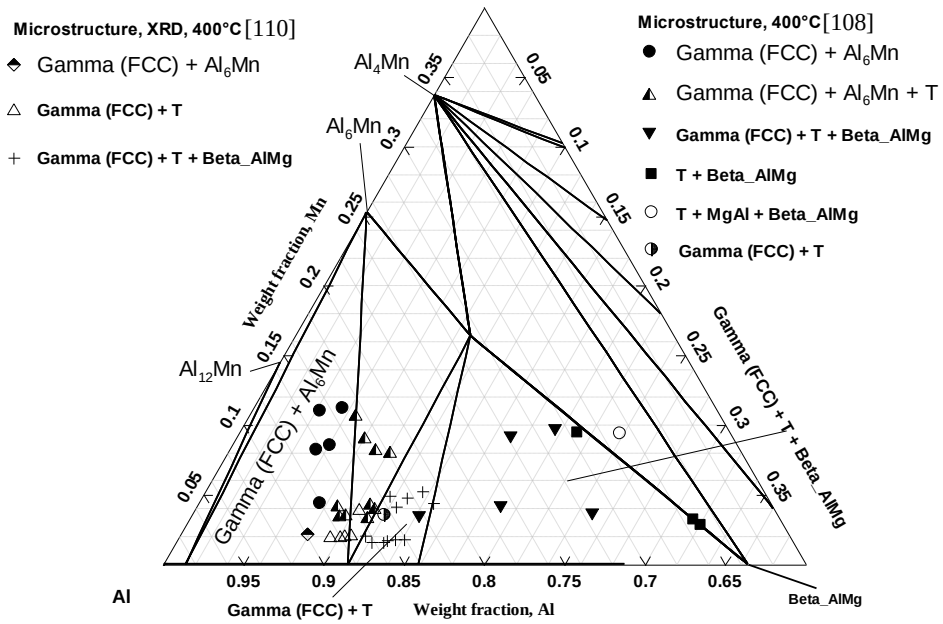

Fig 4.17. Calculated isothermal section at 400°C compared with the experimental data of [108,110]

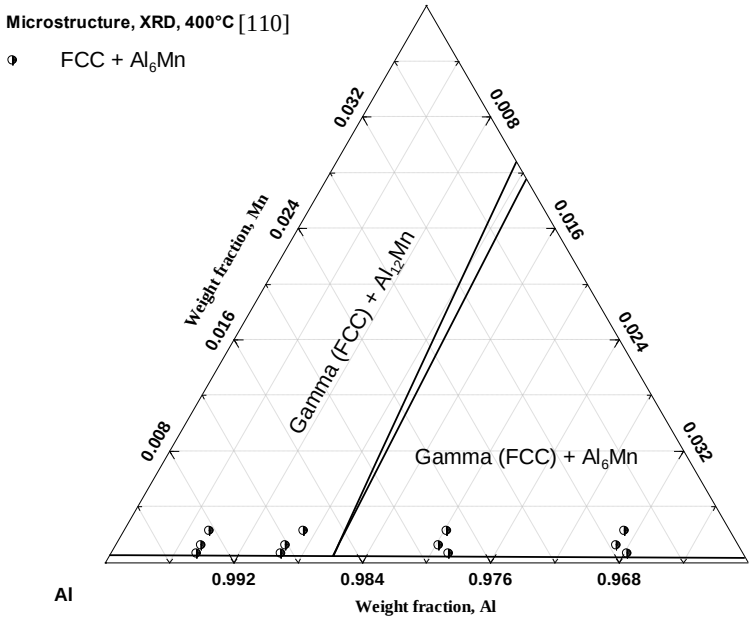

Fig 4.18. Calculated isothermal section in the Al-rich corner at 400°C compared with the experimental data of [110]

Another isothermal section at 450°C has been compared with the data of [110] in figure 4.19 which shows reasonable agreement. The deviations of the calculated results from the experimental data, as can be seen in figures 4.17 to 4.19, are acceptable considering the possible uncertainties in the measurements.

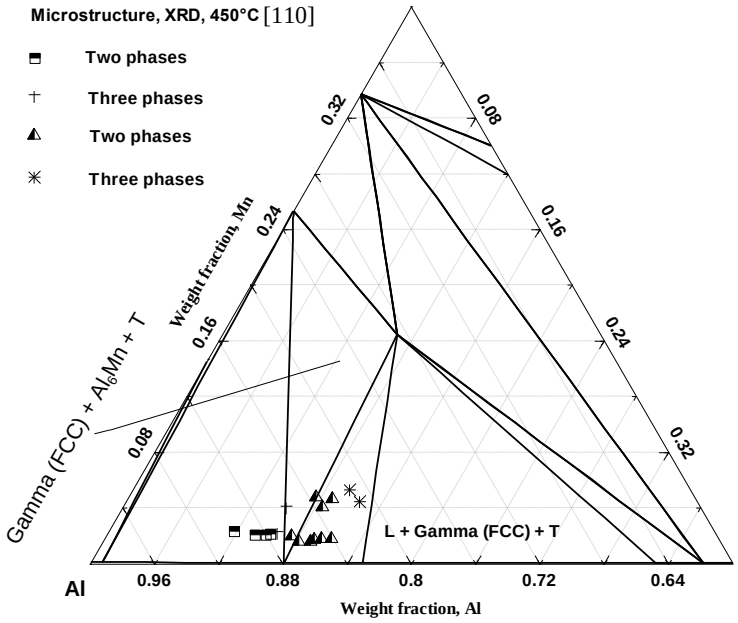

Fig 4.19. Calculated isothermal section in the Al-rich corner at 450°C compared with the experimental data of [110]

Calculated isothermal sections at 670°C, 700°C, 710°C and 730°C have been compared with the available experimental data of [99-103] in figures 4.20 to 4.23. A good agreement has been achieved in all these calculations. It should be noted here that the isothermal section at 700° C in figure 4.21 has been drawn on a rectangular coordinates instead of triangular in order to enable better viewing and comparison with the experimental data. Although, Nelson [99] and Mirgalovskaya et al. [100] and Simensen et al. [101,102] did not report the equilibrium phases, figures 4.21 and 4.23

show that their liquidus isotherms are well reproduced by the current model. The experimental liquidus isotherms of [103] are also reproduced in the calculations as can be seen in figures 4.20, 4.21 and 4.23.

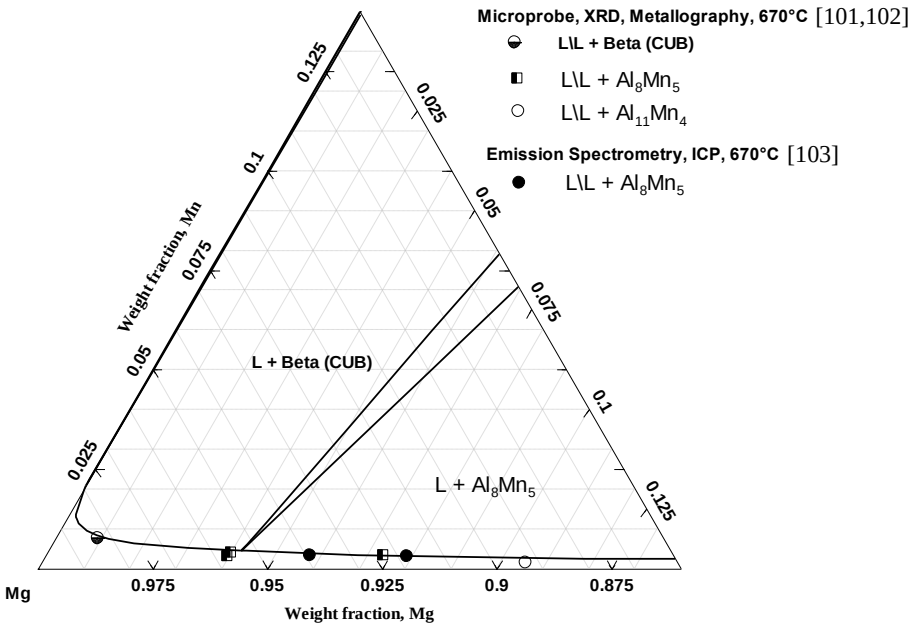

Fig 4.20 Calculated isothermal section in the Mg-rich corner at 670°C compared with the experimental data of [101-103]

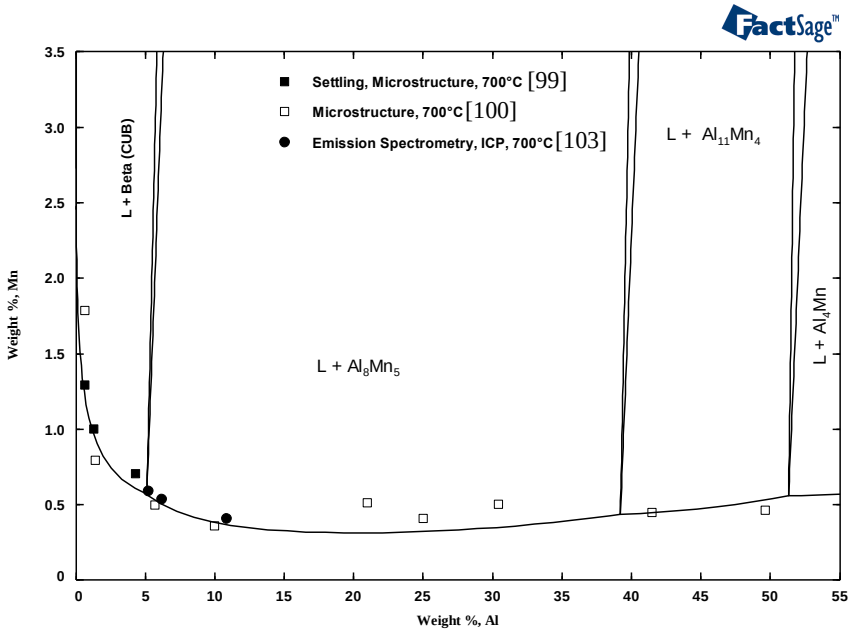

Fig 4.21 Calculated isothermal section in the Mg-rich corner at 700°C compared with the experimental data of [98,99,102] (data represents liquidus isotherms)

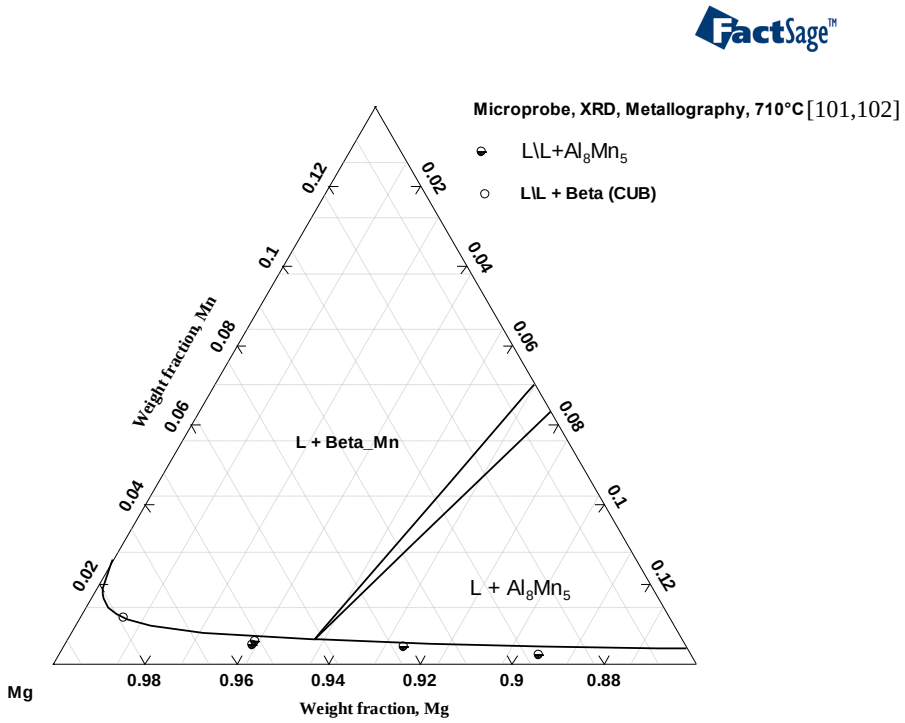

Fig 4.22 Calculated isothermal section in the Mg-rich corner at 710°C compared with the experimental data of [101,102]

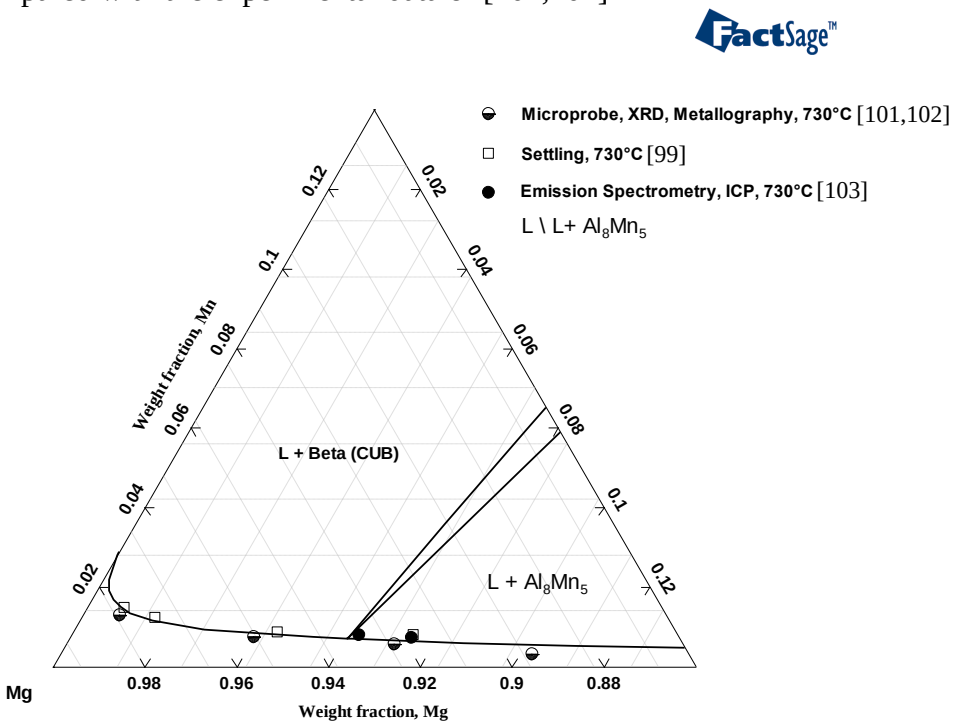

Fig 4.23 Calculated isothermal section in the Mg-rich corner at 730°C compared with the experimental data of [99,101-103]

The calculated isothermal section at 850°C in figure 4.24 which is drawn on a rectangular coordinates also shows reasonable agreement with the data of [100] which could not be satisfactorily reproduced with the models of Ohno and Schmid-Fetzer [97] and Shukla and Pelton [30].

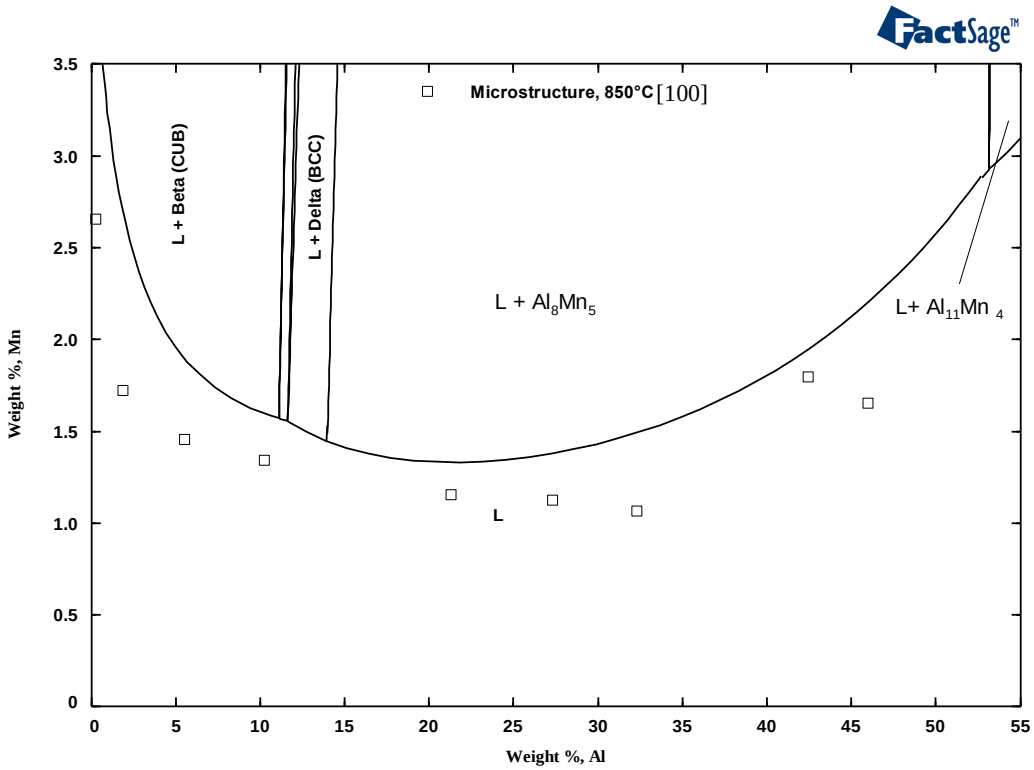

Fig 4.24 Calculated isothermal section in the Mg-rich corner at 850°C compared with the experimental data of [100] (data represents liquidus isotherm)

The solubility of Mn in the liquid Mg-Al alloys has been compared with the experimental data of [99] and [103] in figures 4.25 and 4.26, respectively.

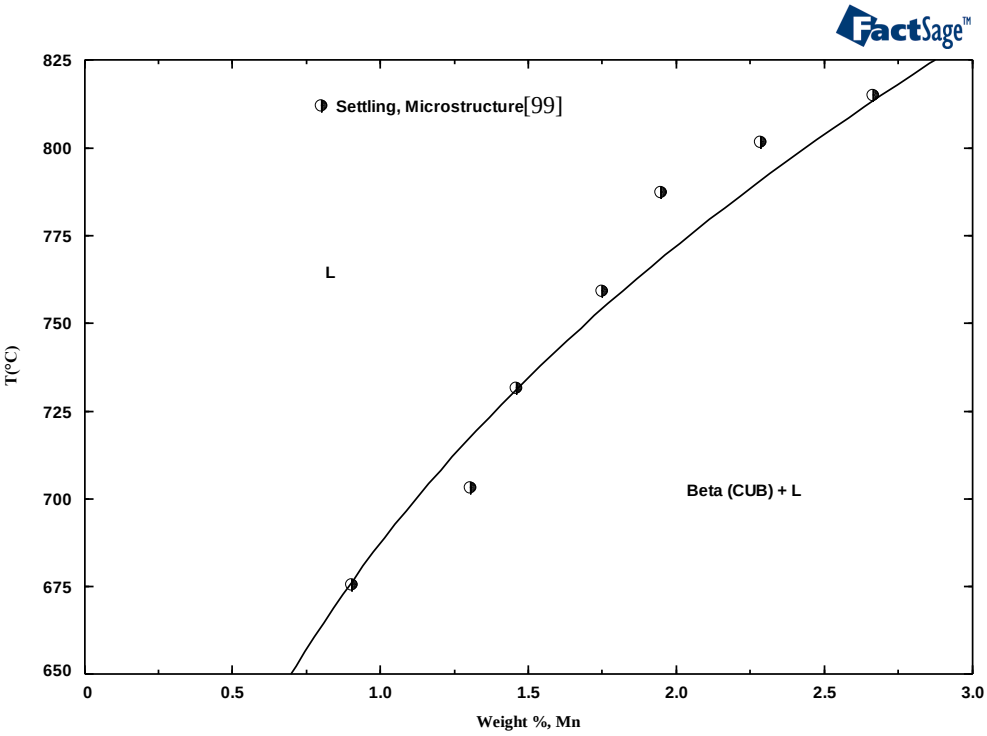

Fig 4.25 Calculated vertical section with 0.8 wt% Al, compared with the experimental data of [99]

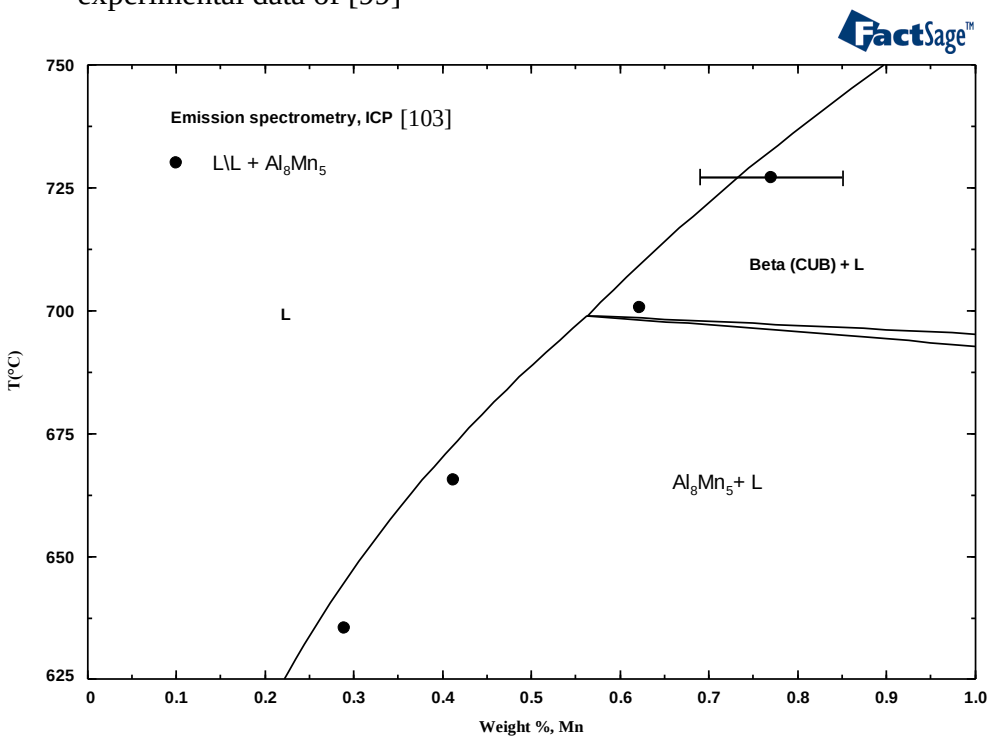

Fig 4.26 Calculated vertical section at 5.05 wt% Al compared with the experimental data of [103]

Figure 4.25 shows that, the data of Nelson [99] are in accordance with the current calculation although he did not report the type of the equilibrium phases. However, there is a disagreement in the identification of equilibrium phase between the current calculation and two data points of Thorvaldsen and Aliravci [103] as can be seen in figure 4.26. These two data points were reported to be in the Al_8Mn_5 phase region by Thorvaldsen and Aliravci [103] who used emission spectrometry and ICP technique with 0.01 wt% repeatability for manganese and 0.1-0.2 wt% for aluminum, while this calculation detects this as Beta (CUB) region. They [103] proposed a solubility model fitting these chemical analysis data. However, their solubility model did not reproduce the data in the low Al concentrations (≈ 5 wt %) region specially those resulted from high holding temperature (>700°C) experiments. The deviations of compositions in this region could not be explained by the repeatability of the ICP analyses. They [103] considered the possibility of precipitation of different equilibrium phase than Al_8Mn_5 in this region as the most likely cause for the deviations from their solubility model. Their observation together with the results of Nelson [99] and Simensen et al. [101,102] suggest that the equilibrium phase in this high temperature and low aluminum concentration region is probably the Beta (CUB) phase. This agrees with the current calculation in this region as shown in figure 4.16. Further, the error bar in this figure indicates that the current calculation is within the error limits of Thorvaldsen's et al. measurements [103].

The calculated solubilities of Mn and Mg in solid Gamma (FCC) phase at different temperatures are compared with the available experimental measurements of Fahrenhorst and Hoffman [18] in figure 4.27. The calculations are consistent with the experimental data as can be seen in the figure.

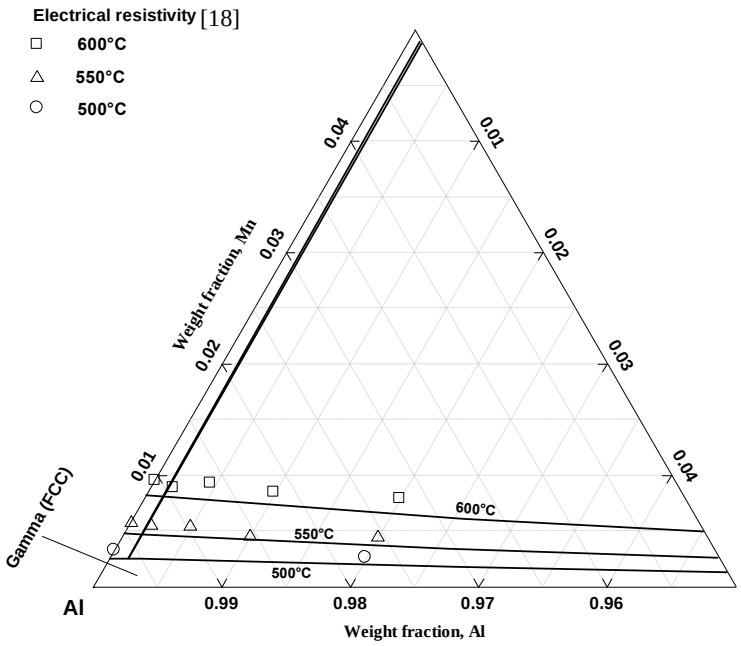

Fig 4.27 Calculated solubilities of Mn and Mg in Gamma (FCC) phase compared with the experimental data of [18]

4.6 Mg-Mn-Zn System

A simple extrapolation of the Mg-Mn, Mg-Zn and Mn-Zn system to construct the ternary Mg-Mn-Zn has been carried out using the Kohler [127] extrapolation technique without the use of any ternary interaction parameter. The extrapolated liquidus projection is shown in figure 4.28 for the entire composition region. The calculated primary phase regions are shown with the arrows indicating the descending temperature directions. The Zn-rich corner of the liquidus projection has been zoomed and the invariant reactions and critical points are shown in figure 4.29. Table 4.10 lists the temperature, reaction types and the composition of these calculated invariant points.

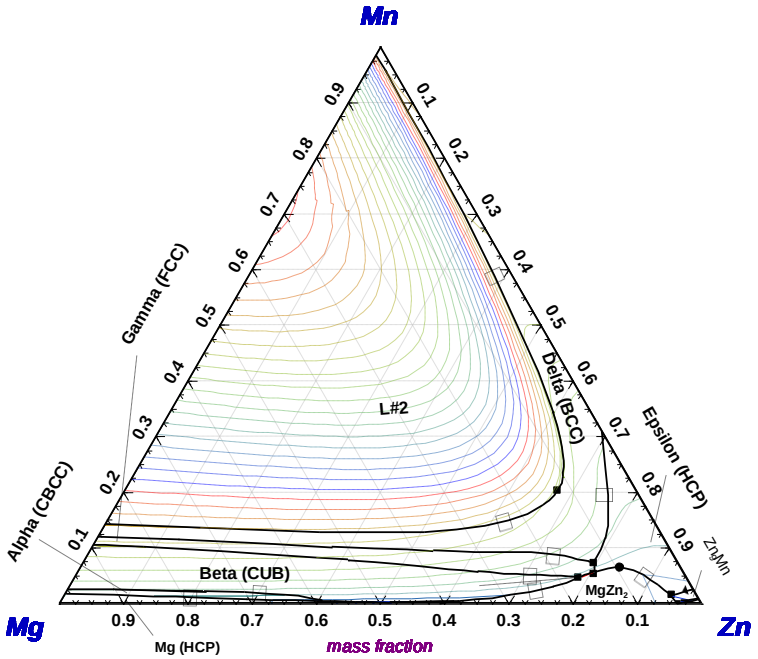

Fig 4.28 Calculated liquidus projection of the Mg-Mn-Zn system with arrows indicating the decreasing temperature directions (Dotted lines are isotherms)

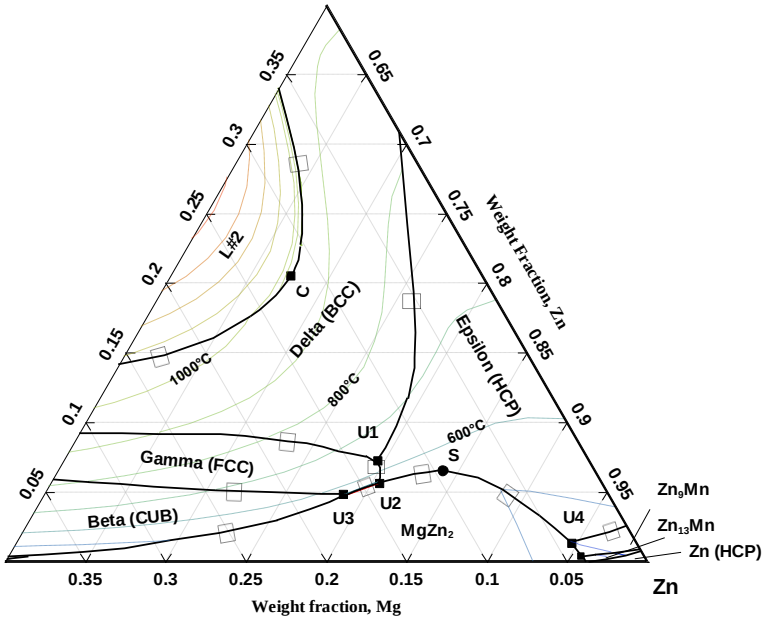

Fig 4.29 Liquidus projection in the Zn-rich corner of the Mg-Mn-Zn system (Dotted lines are isotherms)

Table 4.10 Calculated invariant reactions and critical points in the Mg- Mn –Zn system

Reaction	T (°C)	Type *	Composition (wt %)		
			Mn	Mg	Zn
L#1 + Delta (BCC) ⇔ Gamma (FCC) + Epsilon (HCP)	628	U1	7.4	13.0	79.6
L#1 + Epsilon (HCP) ⇔ Gamma (FCC) + $MgZn_2$	569	U2	5.8	14.0	80.2
L#1 + Gamma (FCC) ⇔ Beta (CUB) + $MgZn_2$	567	U3	5.2	16.4	78.4
L#1 + Epsilon (HCP) ⇔ $MgZn_2$ + Zn_9Mn	400	U4	1.9	3.9	94.2
L#1 ⇔ $MgZn_2$ + Epsilon (HCP)	552	S	6.5	9.6	83.9
L#1 + L#2 ⇔ Delta (BCC)	966	C	20.5	12.1	67.4

* U: Transition type * S: Saddle point * C: Consolute point

The other invariant reactions are degenerate of those from the Mg-Zn binary edge. At the middle of the diagram, the invariant reactions are calculated and shown in figure 4.30 for better illustration.

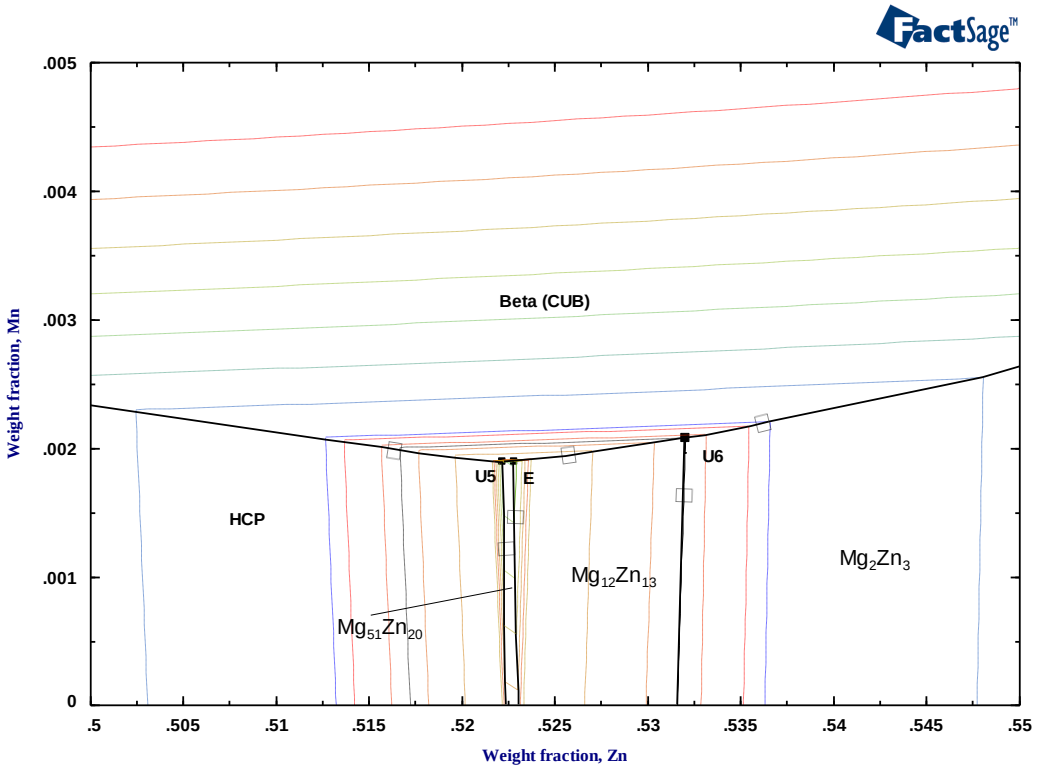

Fig 4.30 Liquidus projection near the Mg-Zn binary edge showing the almost degenerated invariant reactions (Dotted lines are isotherms)

The calculated invariant points shown in figure 4.30 are listed in table 4.11 and compared with the calculated results of [13].

Table 4.11 Calculated invariant points in the Mg-Mn-Zn system near the binary Mg-Zn edge compared with the calculation of [13]

Reaction	T (°C)	Type*	Composition (wt %)			
			Mn	Mg	Zn	Ref
L#1 + Mg (HCP) ⇔ Beta (CUB) + $Mg_{51}Zn_{20}$	340.18	U	0.2	47.6	52.2	This work
	340.18	U	0.2	47.5	52.3	[13]
L#1 + Mg_2Zn_{13} ⇔ Beta (CUB) + $Mg_{12}Zn_{13}$	346.85	U	0.2	46.6	53.2	This work
		-	-	-	-	-
L#1 + ⇔ Beta (CUB) + $Mg_{51}Zn_{20}$ + $Mg_{12}Zn_{13}$	340.16	E	0.2	47.5	52.3	This work
	340.16	E	0.2	47.4	52.3	[13]

* U: Transition type * E: Ternary eutectic

In figures 4.31 through 4.35, several isothermal sections where experimental data points are reported by [11] have been calculated and compared.

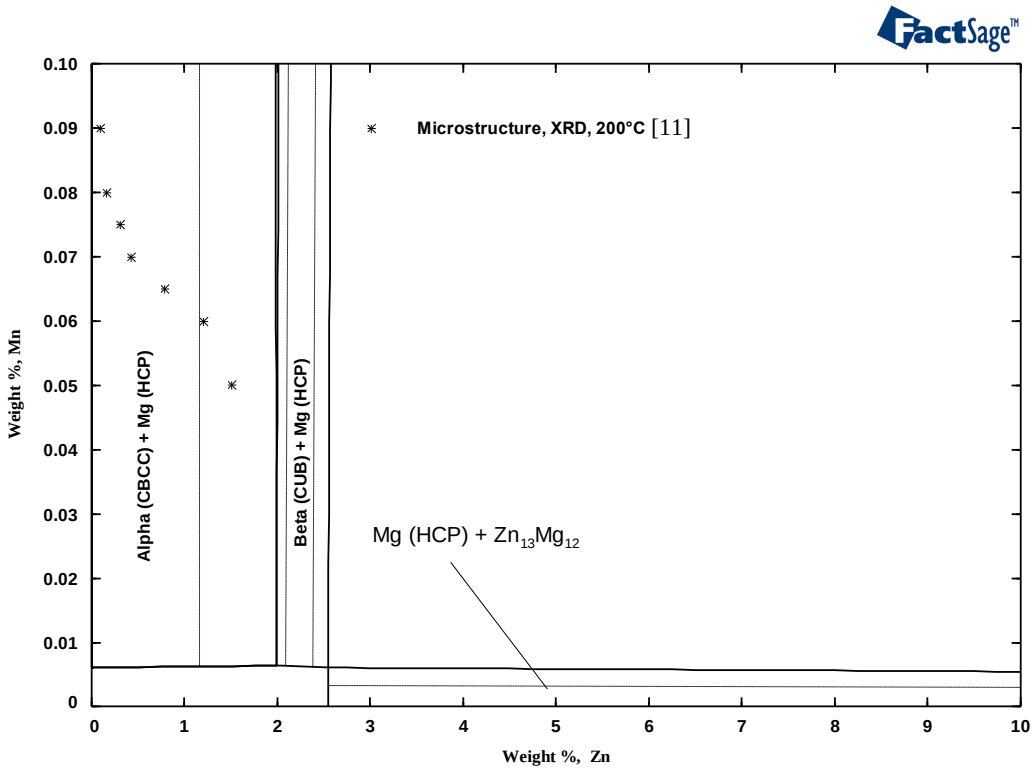

Fig 4.31 Isothermal section of the Mg-rich corner at 200°C in the Mg-Mn-Zn system compared with the experimental results of [11] (dotted lines are two-phase tie-lines)

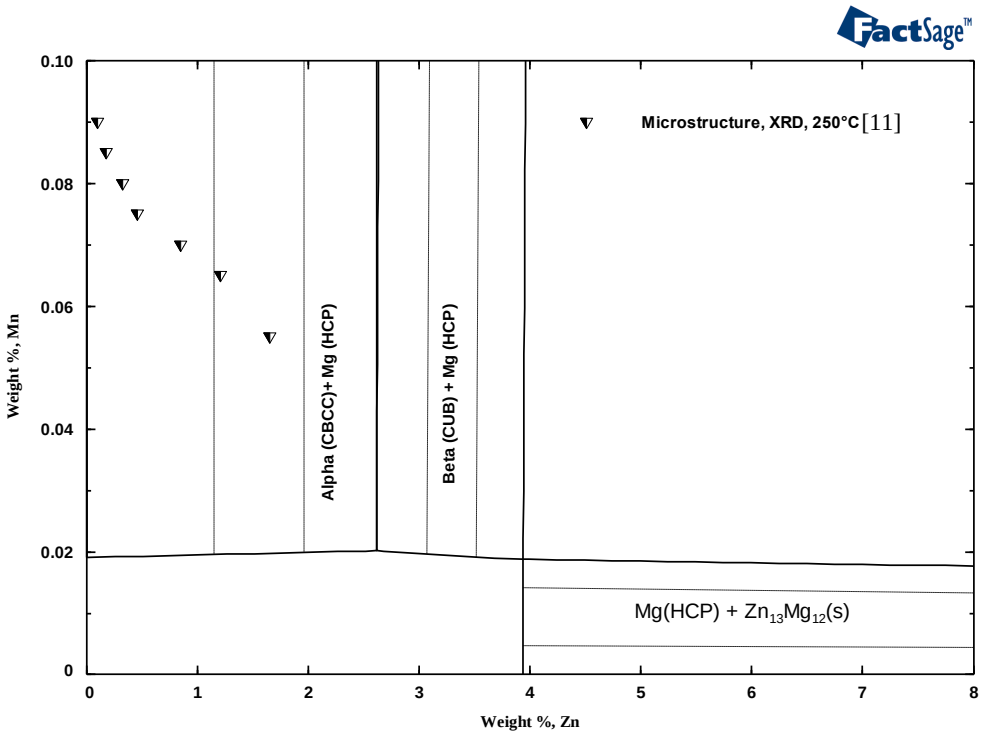

Fig 4.32 Isothermal section of the Mg-rich corner at 250°C in the Mg-Mn-Zn system compared with the experimental results of [11] (dotted lines are two-phase tie-lines)

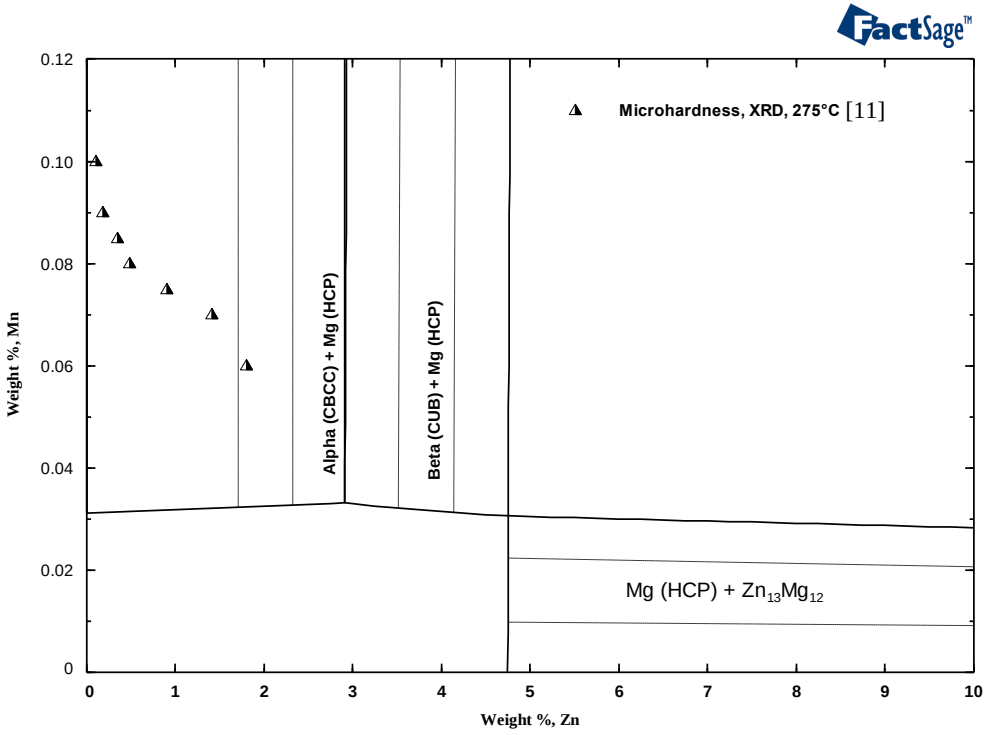

Fig 4.33 Isothermal section of the Mg-rich corner at 275°C in the Mg-Mn-Zn system compared with the experimental results of [11] (dotted lines are two-phase tie-lines)

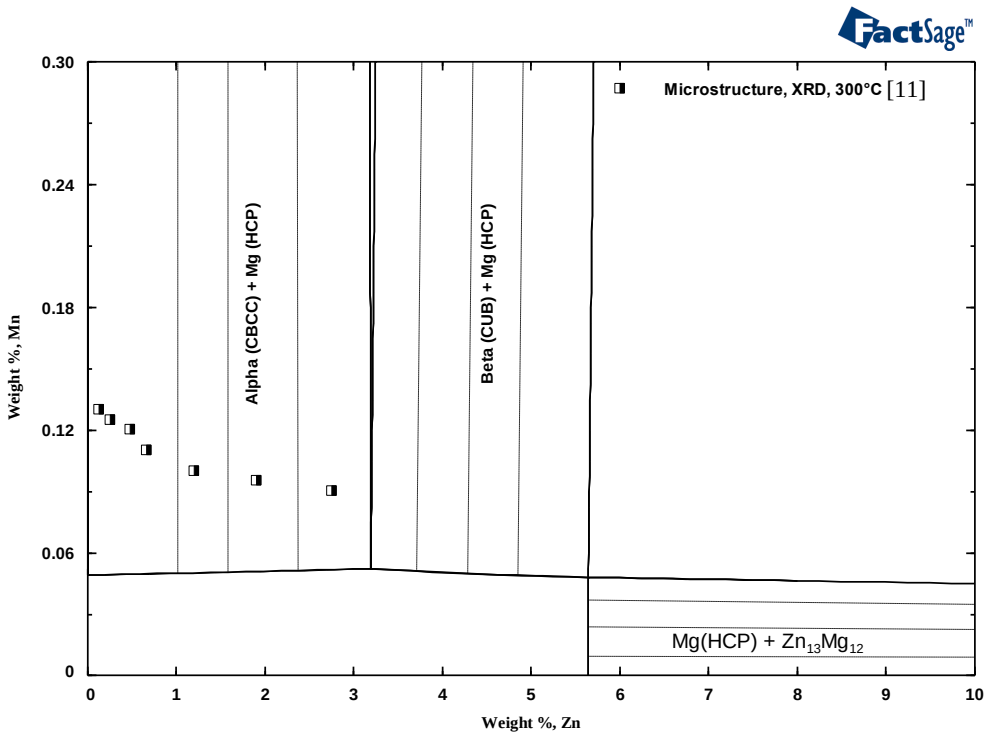

Fig 4.34 Isothermal section of the Mg-rich corner at 300°C in the Mg-Mn-Zn system compared with the experimental results of [11] (dotted lines are two-phase tie-lines)

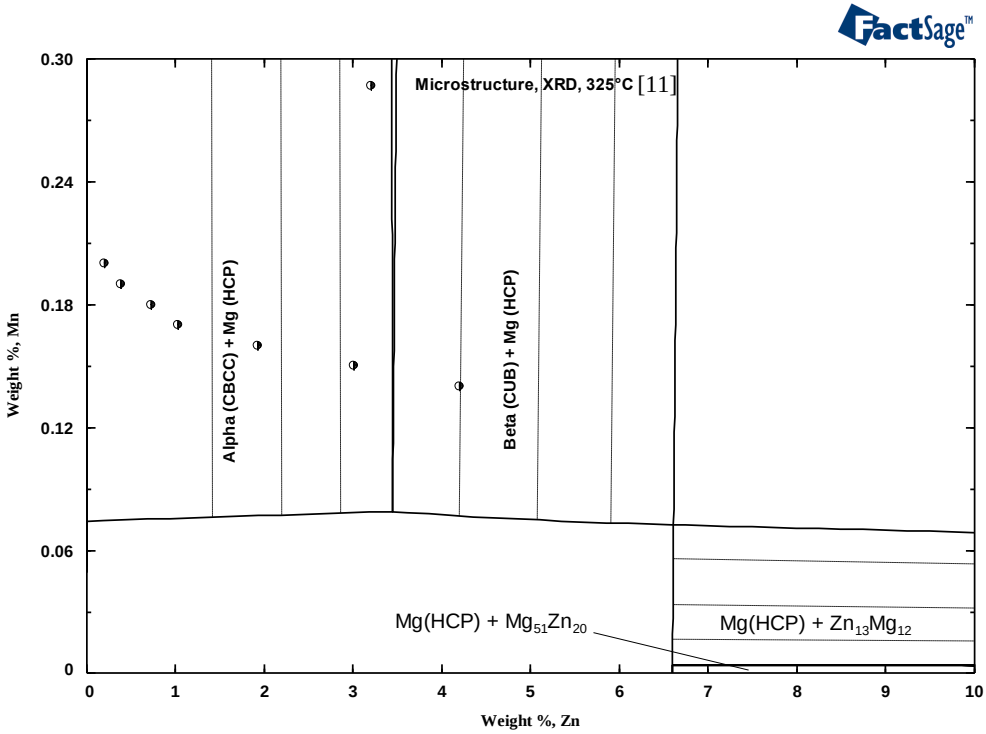

Fig 4.35 Isothermal section of the Mg-rich corner at 325°C in the Mg-Mn-Zn system compared with the experimental results of [11] (dotted lines are two-phase tie-lines)

It should be noted here that the figures above have been drawn on two dimensional coordinates to enable better viewing and comparison. It can be seen form these figures that the calculation always estimates lower solubility than observed in the experimental results of [11] who measured the solubilities by microstructural analysis. As discussed in [13], detecting trace compositions in small sized particles by microstructural observation is often associated with high difficulties and this may have caused observing higher solubilities than the actual values. Further, when the weight fraction of Zn approaches zero, the experimental observation by [11] does not approach to the solubility limit of the Mg-Mn binary system as pointed out in [13]. Although the data of [12] provides quantitatively different results than [11], agreement was found in the observed trend of solubility behavior of Mn in Mg-Zn alloys indicating that the Mn solubility in Mg (HCP) decreases with increasing Zn composition. Ohno and Schmid-Fetzer [13] questioned this consistency suspecting it to be the result of possible non-equilibrium effect in these two experimental works. The current calculation estimates almost constant solubility of Mn in Mg (HCP) with the increase of Zn composition similar to the calculated results of [13].

CHAPTER 5

Conclusions, Original Contribution and Recommendations

5.1 Conclusions

In the current work, three binary and two ternary systems have been modeled using CALPHAD approach. All the experimental phase equilibria and thermodynamic data for the Mg-Mn, Al-Mn and Mn-Zn binary systems and the Mg-Al-Mn and Mg-Mn-Zn ternary systems have been collected and evaluated in terms of their reliablity. Suitable models have been chosen for each of the stable phases in the systems. The modified quasichemical model has been used for the liquid phase and epsilon (HCP) phase in the Mn-Zn system. Substitutional solution model is used for modeling the terminal solid solutions and the intermediate delta (BCC) and epsilon (HCP) phases in the Al-Mn system. The intermediate solid solutions Al_8Mn_5 in the Al-Mn system and Zn_8Mn_5 in the Mn-Zn system are modeled using the compound energy formalism, with three and two sublattices, respectively. Besides, the stable line compounds are modeled as stoichiometric phases. The current model of the Al-Mn, Mg-Mn, Mn-Zn and Mg-Al-Mn systems has extensively been verified by the representative experimental information. In most of the cases, all the current calculations have been found consistent with the experimental observations. Some discrepancies with a few of the experimental data in the Mg-Al-Mn system have been observed. However, the deviations of the current

calculations from the experimental information are acceptable considering the uncertainties of the experiments such as the experimental error limits, probable sample contamination or other experimental conditions. The calculated Mg-Mn-Zn system could not be verified by experimental data from the literature because the few available experimental data (two sets) may not represent the actual equilibrium condition as discussed in section 2.6. Nevertheless, the current calculation is found consistent with other available calculation. Further, the current model of the Al-Mn system is compared with the most recent work on this sytem that also uses the MQC model for the liquid phase. The comparison reveals that A better agreement with the experimental data with less number of model parameters has been achieved in the current work. In the absence of experimental data, significant contradictions were found in the calculations of the other existing models predicting the critical temperature of the liquid miscibility gap in the Mg-Mn system. The calculated critical temperature of the liquid miscibility gap with the current model is found consistent with the estimated value using the available empirical equation. In addition to this, some thermodynamic quantities in the Mg-Mn system are compared with other similar systems and found reasonably comparable. The current model of the Mn-Zn system covers a wide temperature range starting from room temperature and shows a better agreement with the experimental data compared with the previous work on this system. Above all, the current thermodynamic model of the binary and ternary systems can represent all the reliable experimental phase equilibria and thermodynamic data in a self-consistent manner. Nevertheless, scope for improvement in the developed database always exist with the advent of new experimental information.

5.2 Original Contribution

This work offers a reliable thermodynamic model for three binaries and two ternaries; Mg-Mn, Al-Mn, Mn-Zn, Mg-Al-Mn and Mg-Mn-Zn systems. This is the first attempt to model the Mn-Zn and Mg-Mn-Zn systems using MQC model which is scientifically more reliable in terms of better predictability of the higher order system properties compared with the BW random mixing model. Thus, MQC model is also used for describing the liquid in each of the binary and ternary systems and epsilon (HCP) phase in Mn-Zn system. The optimized model parameters are capable of reproducing all the reliable phase diagram and thermodynamic data in each systems. The model can be used to design key experiments and contribute to the subsequent improvement of the descriptions of the system. The thermodynamic descriptions of the binary and ternary systems can be combined with other similar descriptions of different systems to form a consistent multicomponent database which is the ultimate purpose of this effort in a broad aspect. The current work, thus, offers a significant contribution to the development of a reliable Mg multicomponent thermodynamic database.

5.3 Recommendations for Future Work

There is a scope of providing new experimental data for verifying the results of the current thermodynamic modeling by carrying out some key experiments where sufficient data are not available. The experiments can be designed on the basis of the current modeling of the systems. Specifically, it would be a significant contribution if some thermodynamic properties are measured in the Mg-Mn system as no experimental thermodynamic data on this binary could be found in the literature. Also, the phase

equilibria in the Mn-Zn system needs to be verified more precisely as there still exists some ambiguity regarding the probable separation of the intermediate epsilon(HCP) phase and the correct phase equilibria at temperatures below 400°C. Further, few key experiments in the Mg-Mn-Zn ternary systems based on the current thermodynamic modeling can contribute to the verification of the model and subsequent improvement of the understanding of the equilibrium in this system.

References

[1] M. Aljarrah, Thermodynamic Modeling and Experimental Investigation of the Mg-Al-Ca-Sr System, Ph.D. Thesis, Concordia University, Montreal, Quebec, Canada, 2008

[2] Sk. Rahman, Thermodynamic Modeling of the (Mg, Al)-Ca-Zn Systems, Masters Thesis, Concordia University, Montreal, Quebec, Canada, 2008

[3] A. Pelton, S. Degterov, G. Eriksson, C. Robelin and Y. Dessureault, The Modified Quasichemical Model I-Binary Solutions, Metall. Mater. Trans. B, 31B (4), 2000, p 651-659

[4] M. Mezbahul-Islam, D. Kevorkov and M. Medraj, The Equilibrium Phase Diagram of the Magnesium-Copper-Yttrium System, J. Chem. Thermodyn., 40 (7), 2008, p 1064-1076

[5] M. Aljarrah and M. Medraj, Thermodynamic Assessment of the Phase Equilibria in the Al-Ca-Sr System using the Modified Quasichemical Model, J. Chem. Thermodyn., 40 (4), 2008, p 724-734

[6] M. Aljarrah and M. Medraj, Thermodynamic Modeling of the Mg-Ca, Mg-Sr, Ca-Sr and Mg-Ca-Sr Systems Using the Modified Quasichemical Model, CALPHAD, 32 (2), 2008, p 240-251

[7] A. Shukla, Y. Kang and A. Pelton, Thermodynamic Assessment of the Si-Zn, Mn-Si, Mg-Si-Zn and Mg-Mn-Si Systems, CALPHAD, 32 (3), 2008, p 470-477

[8] Y. Kang, A. Pelton, P. Chartrand and C. Fuerst, Critical Evaluation and Thermodynamic Optimization of the Al-Ce, Al-Y, Al-Sc and Mg Sc Binary Systems, CALPHAD, 32 (2), 2008, p 413-422

[9] X. Liu, R. Kainuma, H. Ohtani and K. Ishida, Phase Equilibria in the Mn-rich Portion of the Binary System Mn-Al, J. Alloys Compd., 235 (2), 1996, p 256-261

[10] X. Liu, R. Kainuma and K. Ishida, Thermodynamic Assessment of the Aluminum-Manganese (Al-Mn) Binary Phase Diagram, J. Phase Equilib., 20 (1), 1999, p 45-56

[11] F. Bumazhnov, Physichochemical Investigation at Varied Temperatures of Solubility of Zinc and Manganese in Magnesium, Izvestiya Vysshikh Uchebnykh Zavedenii, Tsvetn. Met. (Moscow), 2 (6), 1960, p 138-143

[12] H. Joel and A. Schneider, Magnesium-Manganese-Zinc (-Silicon-Titanium) Alloy, Metall, 22 (3), 1968, p 193-199

[13] M. Ohno and R. Schmid-Fetzer, Mg-rich Phase Equilibria of Mg - Mn - Zn Alloys Analyzed by Computational Thermochemistry, Int. J. Mat. Res., 97 (5), 2006, p 526-532.

[14] A. McAlister and J. Murray, the (Al-Mn) Aluminum-Manganese System, Bull. Alloy Phase Diag., 8 (5), 1987, p 438-447

[15] M. Drits, E. Kadaner, E. Padezhnova and N. Bochvar, Determination of the Limits of Mutual Solubility of Manganese and Cadmium in Solid Aluminum, Zh. Neorg. Khim., 9 (6), 1964, p 1397-1402

[16] E. Dix, W. Fink and L. Willey, Equilibrium Relations in Aluminum-Manganese Alloys of High Purity. II, Trans. Am. Inst. Mining Met. Eng., 104, 1933, p 335-352

[17] E. Butchers and W. Hume-Rothery, The Solubility of Mn in Al, J. Inst. Met., 71 (985), 1945, p 87-91

[18] E. Fahrenhorst and W. Hofmann, The Solubility of Manganese in Aluminum Containing up to 2% Magnesium, Metallwissenschaft, 19, 1940, p 891-893

[19] I. Obinata, K. Yamaji, and E. Hata, Subcooled Aluminum-Manganese Alloys. I, Nippon Kinzoku Gakkaishi, 17, 1953, p 496-501

[20] C. Bale, A. Pelton and W. Thompson, Factsage thermochemical software, http://www.factsage.com

[21] K. Kumar and P. Wollants, Some Guidelines for Thermodynamic Optimisation of Phase Diagrams, J. Alloys and Compd., 320 (2), 2001, p 189-198

[22] A. Jansson, A Thermodynamic Evaluation of the Al-Mn System, Metall. Trans. A, 23 (11), 1991, p 2953-2962

[23] H. Okamoto, Al-Mn (Aluminum-Manganese), J. Phase Equilib., 18 (4), 1997, p 398-399

[24] C. Müller, H. Stadelmaier, B. Reinsch and G. Petzow, Merallurgy of the Magnetic τ-Phase in Mn-Al and Mn-Al-C, Z. Metallkd., 87 (7), 1996, p 594-597

[25] G. Kuznetsov, A. Barsukov and M. Abas, Study of Manganese, Chromium, Titanium, and Zirconium solubility in solid aluminum, Izvestiya Vysshikh Uchebnykh Zavedeni, Tsvetn. Met. (Moscow), 1, 1983, p 96-100

[26] Y. Minamino, Y. Toshimi, H. Araki, N. Takeuchi, Y. Kang, Y. Miyamoto and T. Okamoto, Solid Solubilities of Manganese and titanium in Aluminum at 0.1 MPa and 2.1 GPa, Metall. Mater. Trans. A, 22A (3), 1991, p 783-786

[27] K. Ishida, Summary of the Proceedings of the CALPHAD XXIV Meeting, CALPHAD, 20 (1), 1996, p 1-35

[28] A. Livanov and M. Vozdvizhenskii, Recrystallization of Aluminum Alloys with Manganese, Trudy Moskov. Avaiatsion, 31, 1958, p 65-83

[29] Y. Du, J. Wang, J. Zhao, J. Schuster, F. Weitzer, R. Schmid-Fetzer, M. Ohno, H. Xu, Z. Liu, S. Shang and W. Zhang, Reassessment of the Al-Mn System and A Thermodynamic Description of the Al-Mg-Mn System, Int. J. Mat. Res., 98 (9), 2007, p 855-871.

[30] A. Shukla and A. Pelton, Thermodynamic Assessment of the Al-Mn and Mg-Al-Mn Systems, J. Phase Equilib. Diffus.,:Section I: Basic and Applied Research, in Press

[31] Y.Esin, N. Bobrov, M. Petrushevski and P. Geld, Concentration Variation of the Enthalpies of Formation of Manganese-Aluminum Melts at 1626 K, Zh. Fiz. Khim., 47 (8), 1973, p 1959-1962

[31] G. Batalin, E. Beloboradova, B. Stukalo and A. Chekhovskii, Thermodynamic Properties of Molten Alloys of Aluminum with Manganese, Ukr. Khim. Zh., 38 (8), 1972, p 825-827

[33] R.Chastel, M. Saito and C. Bergman, Thermodynamic Investigation on $Al_{1-x}Mn_x$ Melts by Knudsen Cell Mass Spectrometry, J.Alloys and Compd., 205 (1-2), 1994, p 39-43

[34] O. Kubaschewski and G. Heymer, Heats of Formation of Transition-Metal Aluminides, Trans. Farad. Soc., 56, 1960, p 473-478

[35] S. Meschel and O. Kleppa, The Standard Enthalpy of Formation of Some 3d Transition Metal Aluminides by High-Temperature Direct Synthesis Calorimetry, NATO ASI Ser., Ser. E, 256 (Metallic Alloys), 1994, p 103-112

[36] R. Kematick and C. Myers, Thermodynamics and Phase Equilibria in the Al-Mn System, J. Alloys and Compd., 178 (503 p), 1992, p 343-349

[37] A. Hashemi and J. Clark, the Mg-Mn (Magnesium-Manganese) System, Bull. Alloy Phase Diag., 6 (2), 1985, p 160-164

[38] J. Ruhrmann, Magnesium-Manganese Alloys, quoted by Schmidt, W., Z. Metallkd., 19 (11), 1927, p 452-455

[39] E. Schmid, Contribution to the Physics and Metallography of Magnesium, Z.Electrochem., 37 (8/9), 1931, p 447-459

[40] E. Schmid and G. Siebel, Determination of Solid Solubility of Mn in Mg by X-ray Analysis, Metallwirtschaft, 10 (49), 1931, p 923-925

[41] H. Sawamoto, Equilibrium Diagram of Magnesium-rich Magnesium-Manganese Binary System, Suiyokwai-shi, 8, 1935, p 763-768.

[42] J. Grogan and J. Haughton, Alloys of Magnesium. Part XIV. The Constitution of the Magnesium Rich Alloys of Magnesium and Manganese, J. Inst. Met., 69, 1943, p 241-248

[43] A. Beerwald, On the Solubility of Iron and Manganese in Magnesium and Magnesium-Aluminum Alloys, Metallwissenschaft, Metalltecknik, 23, 1944, p 404-407

[44] N. Tiner, The solubility of Manganese in Liquid Magnesium, Trans. Met. Soc. AIME, 161, 1945, p 351-359

[45] G. Siebel, The Solubility of Iron, Manganese and Zirconium in Magnesium Alloys, Z. Metallkd., 39, 1948, p 22-27

[46] A. Schneider and H. Stobbe-Scholder, The Structure and Technical Preparation of Corrosion-Resistant Magnesium-Manganese Alloys, Metall, 4 (9/10), 1950, p 178-183

[47] D. Petrov, M. Mirgalovskaya, I. Strelnikova and E. Komova, The Constitution Diagram for the Magnesium-Manganese System, Trans. Inst. Met., 1, 1958, p 142-143

[48] M.V. Chukhov, On the Solubility of Mn in Liquid Mg, Legkie Splaavy, Akad. Nauk SSSR, Inst. Met. A.A. Baikova, 1, 1958, p 302-305

[49] M. Drits, Z. Sviderskaya and L. Rokhlin, Solid Solubility of Mn in Mg, Izv. Nauka, 1964, p 272-278

[50] S. Ishida, Mg-Mn and Mg-Mn-Fe Alloys, Rep. Aeronaut. Res. Inst. Tokyo Imp. Univ., 280, 1944, p 397-405

[51] J. Gann, Treatment and Structure of Magnesium Alloys, Trans. Met. Soc. AIME, 83, 1929, p 309-332

[52] G. Pearson, Magnesium-Manganese Alloys, Ind. Eng. Chem., 22 (4), 1930, p 367-370

[53] W. Mannchen, Heat Conductivity, Electric Conductivity and Lawrence Number of Light Alloys, Z. Metallkd., 23, 1931, p 193-196

[54] M. Drits, Z. Sviderskaya and L. Rokhlin, The Nature of the Manganese Phase of Certain Magnesium Alloys, Metalloved. Term. Obrab. Met., 10, 1959, p 33-37

[55] E. Bakhmetev and I. Golovchinev, Does There Exist a Homogeneous Intermetallic Phase in the Magnesium-Manganese System, Acta Phys. Chim. USSR, 2, 1935, p 571-574

[56] E. Bakhmetev and I. Golovchinev, Is an Intermediate Homogeneous Phase Formed in the System Magnesium-Manganese, Zh. Fiz. Khim., 6 (5), 1935, p 597-600

[57] J. Gröbner, D Mirkovic, M. Ohno and R. Schmid-Fetzer, Experimental Investigation and Thermodynamic Calculation of Binary Mg-Mn Phase Equilibria, J. Phase Equilib. Diffus., 26 (3), 2005, p 234-239

[58] Y. Kang, A. Pelton, P. Chartrand, P. Spencer and C. Fuerst, Critical Evaluation and Thermodynamic Optimiation of the Binary Systems in the Mg-Ce-Mn-Y System, J. Phase Equilib. Diffus., 28 (4), 2007, p 342-354

[59] C. Antion, Etude du system Mg-Mn-Y-Gd et Development d'Alliages de Magnesium pour des Applications Structurales a Chaud, These Docteur de L'INPG, Institut National Polytechnique de Grenoble, 2003

[60] H. Okamoto and L. Tanner, The Mn - Zn (Manganese-Zinc) System, Bull. Alloy Phase Diag. 11 (4), 1990, p 377-384

[61] N. Parravano and U. Perret, The Alloys of Zinc and Manganese, Gazz. Chim. Ital., 45 (I), 1914, p 1-6

[62] P. Gieren, Cast Alloys of Zinc with Special Consideration on Their Utilization as Bushing Metals, Z. Metallkd., 11, 1919, p 14-22

[63] P. Siebe, Manganese -Bismuth, Manganese - Zinc and Manganese -Silver Alloys, Z. Anorg. Allgem. Chem., 108, 1919, p 161-183

[64] W. Peirce, Studies on the Constitution of Binary Zinc-base Alloys, Trans. Met. Soc. AIME, 63, 1923, p 767-795

[65] C. Ackermann, The Binary System Manganese – Zinc, Z. Metallkd., 19, 1927, p 200-204

[66] N. Parravano and V. Montoro, Alloys of Zinc and Manganese, Mem. Accad. Italia, Classe Sci. Fis. Mat. e Nat., 1 (4), 1930, p 3-19

[67] N. Parravano and V. Caglioti, Alloys of Zinc and Manganese, Atti della Accademia Nazionale dei Lincei, Classe di Scienze Fisiche, Mate. e Natur., Rendic., 14, 1931, p 166-169

[68] N. Parravano, and V. Caglioti, Structure and Chemical Composition of Some [Manganese-Zinc and Cobalt-Zinc] Alloys, Mem. Accad. Italia, Chim., 3 (3), 1932, p 5-21

[69] N. Parravano and V. Caglioti, Further investigations of the Alloys of Zinc and Manganese, Ric. Sci., 7 (II), 1936, p 223-224

[70] J. Schramm, The System Manganese-Zinc with 0 to 50% Mn, Z. Metallkd, 32 (12), 1940, p 399-407

[71] E. Weisse, A. Blumenthal and H. Hanemann, Results of a Study of Eutectic Zn Alloys, Z. Metallkd., 34, 1942, p 221-221

[72] K. Moeller, X-ray and Microscopic Studies with Quaternary Zn-Mn-Cu-Ag alloys, Z. Metallkd., 35, 1943, p 27-28

[73] G. Edmunds, Liquidus Determinations in Zn-rich Alloys (Zn-Fe; Zn-Cu; Zn-Mn), Trans. Met. Soc., AIME, 156, 1944, p 263-276

[74] E. Potter and R. Huber, Manganese - Zinc Phase Diagram from 0 to 50% Zinc, Trans. Am. Soc. Met., 41, 1949, p 1001-1022

[75] U. Zwicker, γ -Phase of Manganese, Z. Metallkd., 42, 1951, p 246-252

[76] H. Nowotny and R. Bittner, Contribution to the Problem of Anomalous Diamagnetism, Monatsh. Chem., 81, 1950, p 898-901

[77] S. Tezuka, S. Sakai and Y. Nakagawa, Ferromagnetism of Mn - Zn Alloy, J. Phys. Soc. Jpn., 15 (5) 1960, p 931-931

[78] P. Brown, The Structure of the ζ -Phase in the Transition Metal-Zinc Alloy Systems, Acta Cryst., 15, 1962, p 608-612

[79] Y. Nakagawa and T. Hori, Magnetic Transition and Crystal Distortion in MnHg and MnZn3, J. Phys. Soc. Jpn., 17 (8), 1962, p 1313-1314

[80] Y. Nakagawa and T. Hori, Neutron Diffraction Studies of Mn - Zn Alloys, J. Phys. Soc. Jpn., 19 (11), 1964, p 2082-2087

[81] Y. Nakagawa and T. Hori, Phase Diagram of Manganese - Zinc System, Trans. Jpn. Ins. Met., 13 (3), 1972, p 167-170

[82] Y. Nakagawa, S. Sakai and T. Hori, Magnetic Properties of Mn-Zn Alloys, J. Phys. Soc. Jpn., 17 (Suppl. B-I), 1962, p 168-171

[83] B. Henderson and R. Willcox, Lattice Spacing Relations in Hexagonal Close-packed Silver-Zinc- Manganese Alloys, Philos. Mag., 9 (101), 1964, p 829-846

[84] T. Hori and Y. Nakagawa, **A** New Ferromagnetic Phase in Mn-Zn Alloy System, J. Phys. Soc. Jpn., 19 (7), 1964, p 1255-1255

[85] T. Hori and Y. Nakagawa and J. Sakurai, Magnetization and Magnetic Structure of Manganese-Zinc and Manganese-Zinc-Gallium Alloys of Cesium Chlorine-type Structure, J. Phys. Soc. Jpn., 24 (5), 1968, p 971-976

[86] D. Martin, The Specific Heat of Zinc-Manganese Alloys, Ann. Acad. Sci. Fenn., Ser. A, 210, 1966, p 140-140

[87] D. Martin, Specific Heat of Pure Zinc and Some Zinc-Manganese Alloys, Phys. Rev., 167 (3), 1968, p 640-651

[88] D. Martin, Specific Heat of Pure Zinc and Dilute Zinc-Manganese Alloys Below 5.deg.K, Phys. Rev., 186 (3), 1969, p 642-648

[89] E. Wachtel and K.Tsiuplakis, Magnetic Properties of Zinc-rich Zinc-Manganese Alloys in the Liquid and Solid State, Z. Metallkd., 58 (1), 1967, p 41-45

[90] H. Uchishiba, T. Hori and Y. Nakagawa, Cubic -tetragonal Transition and Antiferromagnetism of α'-MnZn3, J. Phys. Soc. Jap., 27 (3), 1969, p 600-604

[91] A. Farrar, and H. King, Axial Ratios and Solubility Limits of Hcp. [Hexagonal Close-Packed] η and ε Phases in the Systems Cadmium-Manganese and Zinc-Manganese, Metallography, 3 (1), 1970, p 61-70

[92] B. Lyazgin, G. Kazantsev, V. Lebedev, I. Nichkov, S. Raspopin and L. Martem'yanov, Thermodynamic Properties of the Manganese-Zinc System, Zh. Fiz. Khim., 45 (8), 1971, p 1976-1978

[93] O. Romer and E. Wachtel, Constitution of the Zinc - Manganese and the Zinc - Manganese -Aluminum Systems, Z. Metallkd., 62 (11), 1971, p 820-825

[94] R. Anantatmula, Brillouin Zone Effects in ζ Phase Alloys of the Manganese - Zinc System, Scr. Metall., 9 (3), 1975, p 223-228

[95] E. Baker, Thermodynamic Activities in the Zinc - Manganese System at 1250° C, Z. Metallkd., 71 (11), 1980, p 760-762

[96] J. Miettinen, Thermodynamic Description of the Cu-Mn-Zn System in the Copper-rich Corner, CALPHAD, 28 (3), 2004, p 313-320

[97] M. Ohno and R. Schmid-Fetzer, Thermodynamic Assessment of Mg-Al-Mn Phase Equilibria, Focusing on Mg-rich Alloys, Z. Metallkd, 96 (8), 2005, p 857-869

[98] N. Ageev, I. Kornilov and A. Khlapova, Magnesium-rich Alloys of the System Magnesium-Aluminum-Manganese, Izvest. Sektora Fiz.-Khim. Anal., 16 (4), 1948, p 130-143

[99] B. Nelson, Equilibrium relations in Magnesium-Aluminum-Manganese Alloys, J. Met., 3, 1951, p 797-799

[100] M. Mirgalovskaya, L. Matkova, and E. Komova, System Magnesium-Aluminum-Manganese, Trudy Inst. Met. im. A. A. Baikova , 2, 1957, p 139-148

[101] C. Simensen, B. Oberlaender, J. Svalestuen and A. Thorvaldsen, The phase diagram for magnesium-aluminum-manganese above 650°C**,** Z. Metallkd. 79 (11), 1988, p 696-699

[102]. C. Simensen, B. Oberlaender, J. Svalestuen and A. Thorvaldsen, Determination of the Equilibrium Phases in Molten Magnesium-4% Aluminum-Manganese Alloys**,** Z. Metallkd., 79 (8), 1988, p 537-540

[103] A. Thorvaldsen and C. Aliravci, Solubility of Manganese in Liquid Mg-Al Alloys, Adv. Prod. Light Met. Met. Matrix Comp., Proc. Int. Symp., 1992, p 277-287

[104] W. Leemann, and H. Hanemann, The System Aluminum-Magnesium-Manganese, Aluminium-Arch, 9, 1940, p 9-10

[105] W. Hofmann, R. Ovrddot. Roentgenographic Methods in the Investigation of Aluminum Alloys, Aluminium, 20, 1938, p 865-872

[106] E. Butchers, G. Raynor and W. Hume-Rothery, The Constitution of Magnesium-Manganese-Zinc-Aluminum Alloys in the Range 0-5 Per Cent Magnesium, 0-2 Per Cent Manganese, 0-8 Per Cent Zinc. I. The Liquidus, J. Ins. Met., 69 (942), 1943, p 209-228

[107] A. Little, G. Raynor and W. Hume-Rothery, The Constitution of Mg-Mn-Zn-Al Alloys in the Range Mg 0-5, Mn 0-2 and Zn 0-8%. III. The 500°C and 400°C Isothermals, J. Ins. Met., 69 (952), 1943, p 423-40

[108] D. Wakeman and G. Raynor, The Constitution of Aluminum-Manganese-Magnesium and Aluminum-Manganese-Silver Alloys, with Special Reference to Ternary-Compound Formation, J. Ins. Met., 75 (1148), 1948, p 131-150

[109] T. Ohnishi, Y. Nakatani and K. Shimizu, Phase Diagram in the Aluminum- Rich Side of the Aluminum-Magnesium-Manganese-Chromium Quaternary System, Keikinzoku, 23 (10), 1973, p 437-443

[110] T. Ohnishi, Y. Nakatani and K. Shimizu, Phase Diagrams and Ternary Compounds of Aluminum-Magnesium-Chromium and Aluminum-Magnesium-Manganese Systems in the Aluminum-Rich Corner, Keikinzoku, 23 (5), 1973, p 202-209

[111] J. Barlock and L. Mondolfo, Structure of Some Aluminum-Iron-Magnesium-Manganese-Silicon Alloys, Z. Metallkd., 66 (10), 1975, p 605-611

[112] G. Raynor, Constitution of Ternary and Some Complex Alloys of Magnesium, Int. Met. Rev., 216, 1977, p 65-96

[113] A. Pelton, "Thermodynamics and Phase Diagrams of Materials" in *Phase Transformation in Materials*, edited by G. Kostorz, Wiley-VCH, 2001, p 1-80

[114] A. Dinsdale, SGTE Data for Pure Elements, Calphad, 15 (4), 1991, p 317-425 (updated 2004 version).

[115] A. Pelton and Y. Kang, Modeling Short-range Ordering in Solutions, Int. J. Mat. Res., 98 (10), 2007, p 1-11

[116] J. Daams, P. Villars and J. Vucht (Editors), Atlas of Crystal Structure Types for Intermetallic Phases, Materials Park, Oh: ASM international, 1991

[117] K. Kumar, I. Ansara and P. Wollants, Sublattice Modelling of the μ-Phase, CALPHAD, 22 (3), 1998, p 323-334

[118] H. Kono, On the Ferromagnetic Phase in Manganese-Aluminum System, J. Phys. Soc. Jpn., 13 (12), 1958, p 1444-1451

[119] R. Schaefer, F. Biancaniello and W. Cahn, Formation and Stability range of the G phase in the Aluminum-Manganese System, Scr. Metall., 20 (10), 1986, p 1439-1444

[120] W. Koster and E. Wachtel, Constitution and Magnetic Properties of Aluminum-Manganese Alloys with More Than 25 At. % Mn, Z. Metallkd., 51, 1960, p 271-280

[121] T. Goedecke and W. Koester, Constitution of the Aluminum-Manganese System, Z. Metallkd., 62 (10), 1971, p 727-732

[122] A. Koch, P. Hokkeling, M.Steeg and K. Vos, New Material for Permanent Magnets on a Base of Mn and Al, J. Appl. Phys., 31 (5), 1960, p 75S-77S

[123] J. Murray, A. McAlister, R. Schaefer, L. Bendersky, F. Biancaniello and D. Moffat, Stable and Metastable Phase Equilibria in the Al-Mn System, Metall. Trans. A, 18A (3), 1987, p 385-392

[124] B. Predel, Constitution and Thermodynamics of Systems with Miscibility Gaps, Z. Metallkd., 56 (11), 1965, p 791-798

[123] R. Singh and F. Sommer, Segregation and immiscibility in Liquid Binary Alloys, Rep. Prog. Phys., 60 (1), 1997, p 57-150

[126] I. Dimov, D. Nenov, N. Gidikova and A. Mosheva, Determination of the Activity of Zinc in Liquid Manganese and Iron Alloys, Arch. Eisenhuett., 48 (4), 1977, p 209-210

[127] F. Kohler, Estimation of the Thermodynamic Data for a Ternary System from the Corresponding Binary Systems, Monats. Chem., 91 (4), 1960, p 738-740